BOREAS An international journal of Quaternary research

A resilient ice cover over the southernmost Mendeleev Ridge during the late Quaternary

TENGFEI SONG, CLAUDE HILLAIRE-MARCEL, ANNE DE VERNAL AND YANGUANG LIU

BOREAS

Song, T., Hillaire-Marcel, C., de Vernal, A. & Liu, Y.: A resilient ice cover over the southernmost Mendeleev Ridge during the late Quaternary. *Boreas*. https://doi.org/10.1111/bor.12632. ISSN 0300-9483.

The presence of a late Quaternary ice sheet/ice shelf over the East Siberian Sea has been proposed in several papers. Here, we further document its duration/resilience based on the sedimentary, bulk mineralogical, and geochemical (organic matter content and its stable isotopic composition, U-Th series) properties of a core raised from the southernmost Mendeleev Ridge. The chronostratigraphy of the studied core was mainly built from the ^{230}Th excess ($^{230}Th_{xs}$) distribution and decay downcore. At the core-top, peaking $^{230}Th_{xs}$ values during the early MIS 3 and mid-MIS 1 encompassing an MIS 2 hiatus were observed. As documented in several papers, these peaks suggest seasonally open ice conditions over proximal continental shelves. Below, the interval spanning MIS 4 and possibly MIS 5d records major ice-rafting events illustrated by overall high coarse-fraction contents. Underlying MIS 5e, down to MIS 11, the sediment depicts relatively low sand (1.7±2.5 dw%), high clay (33.5±4.7 dw%), and very low organic carbon (0.10±0.06 dw%) contents, and low $\delta^{13}C_{org}$ values (−24.3±0.9‰). This section is interpreted as recording fine sediment transport by deep currents and/or meltwater plumes below a resilient ice cover, only interrupted by a few short-duration events. These events include (i) detrital carbonate pulses assigned to deglacial events along the NW Laurentide Ice Sheet margin (Termination (T) III), and (ii) intervals with some planktonic foraminifer occurrences, likely relating to their advection from open areas of the Arctic Ocean (MIS 5e, 9 and 11). All Terminations, but TII and the early MIS 3, show peaking Mn/Al values linked to the submergence of Arctic shelves under a rising sea level. We conclude that the resilient ice cover, likely an ice shelf, has been present over the southern Mendeleev Ridge during most of the interval after the Mid-Pleistocene Transition and was favoured by the low summer insolation of the MIS 14 to 10 interval.

Tengfei Song (song.tengfei@outlook.com), Claude Hillaire-Marcel and Anne de Vernal, Geotop, Université du Québec à Montréal, C.P. 8888, Montréal, QC H3C 3P8, Canada; Yanguang Liu, Key Laboratory of Marine Geology and Metallogeny, First Institute of Oceanography, Ministry of Natural Resources, Qingdao 266061, China and College of Earth Science and Engineering, Shandong University of Science and Technology, Qingdao 266590, China; *received 3rd October 2022, accepted 21st July 2023.*

The existence of ice shelves in the Arctic Ocean has been proposed for more than one century (e.g. Thomson 1888). Based on the observations of glacial scouring and glacigenic landforms on the sea floor of the Lomonosov Ridge, Northwind Ridge, Chukchi Plateau, and Chukchi Rise, Polyak *et al.* (2001) proposed that a 1-km-thick ice shelf covered the Arctic Ocean during the Pleistocene glaciations. This finding was supported by the sea floor mapping at the Arlis Plateau and southern Mendeleev Ridge (e.g. Jakobsson *et al.* 2010, 2016). Recently, the presence of an ice sheet anchored over the East Siberian shelves was further proposed based on the observations of glacial scours with multiple orientations (e.g. Niessen *et al.* 2013; Dove *et al.* 2014) and a glacial trough on the East Siberian–Chukchi seas margin (O'Regan *et al.* 2017), with supporting ice model simulations (Gasson *et al.* 2018; Batchelor *et al.* 2019). Using a 3D thermo-mechanical ice-sheet model, Colleoni *et al.* (2016) suggested that the hypothesized ice body that expanded over the East Siberian continental margin might have been an ice shelf. Although the East Siberian Ice Sheet scenario has been adopted in several studies to decipher the environmental and sedimentation changes in the western Arctic Ocean (e.g. Dong *et al.* 2017, 2020; Ye *et al.* 2020; Wang *et al.* 2021; Alatarvas *et al.* 2022; Zhao *et al.* 2022), arguments against the presence of a grounded ice sheet over the East Siberian shelves have been posed in several studies (e.g. Sher 1995; Brigham-Grette 2013) and have been supported by field investigations (Gualtieri *et al.* 2003; Nørgaard *et al.* 2023). Considering the low precipitation rate over the Arctic during glacials (Kageyama *et al.* 2021), which did not allow the formation of an ice sheet over the areas around the East Siberian Sea (Brigham-Grette 2013), the East Siberian Ice Shelf (henceforth ESIS) scenario appears more likely and is accepted in this study. The presence of an ESIS, either as an extension of the Beringia ice cap (Colleoni *et al.* 2016) or an ice body fed by the ice floes from the Laurentide Ice Sheet (LIS) (Engels *et al.* 2008; Jakobsson *et al.* 2008), could have led to the glacial scouring over the Northwind Ridge and Chukchi Sea Borderland areas (Polyak *et al.* 2001; Niessen *et al.* 2013).

The age and duration of the ESIS, with or without being related to an ice sheet, have not been determined with certainty yet. Its prevalent assignment to Marine Isotope Stage (MIS) 6 and/or MIS 4 (e.g. O'Regan *et al.* 2017; Alatarvas *et al.* 2022) was mainly based on equivocal ecostratigraphical inferences (e.g. Jakobsson *et al.* 2001; Backman *et al.* 2009). One of the ecostratigraphical markers is the coccolith *Emiliania huxleyi*, used with an MIS 5e assignment (Backman *et al.* 2009; Jakobsson *et al.* 2010, 2016), although the first appearance of this

DOI 10.1111/bor.12632

species dates from MIS 8 (Thierstein *et al.* 1977), and probably earlier (Guballa & Peleo-Alampay 2020). The other ecostratigraphical marker is the benthic foraminifer *Bulimina aculeata* used as the datum for the MIS 5a in several studies (e.g. Baumann 1990; Jakobsson *et al.* 2001; Backman *et al.* 2004; Polyak *et al.* 2004; Nørgaard-Pedersen *et al.* 2007), despite the common occurrence of the species since the Miocene (Hayward *et al.* 2004; Tzevahirtzian *et al.* 2023). Besides, discontinuous microfossil records (Backman *et al.* 2009) and potential benthic mixing processes (Hillaire-Marcel *et al.* 2022b) can lead to some biases in the interpretation of microfossil records. The usage of microfossils as stratigraphical tools in the central Arctic Ocean is then questionable.

Recent geophysical investigations from the East Siberian Sea, Chukchi Sea Rise, and the Northwind Ridge have documented the existence of several glacial erosion phases during the Quaternary (Dove *et al.* 2014; Kim *et al.* 2021). The latest deep ice grounding event was assumed to date back to the MIS 4/3 transition based on the Mn-based cyclostratigraphy time frame and the identification of Pink-White (PW) layers (Schreck *et al.* 2018; Joe *et al.* 2020). With a similar age model, clay mineral and geochemical studies of sedimentary sequences from the Mendeleev and Northwind ridges, and the Canada Basin also illustrated the development of the ESIS during the last two glacial episodes (e.g. Dong *et al.* 2017, 2020; Ye *et al.* 2020). However, radiometric-based chronostratigraphies (Not & Hillaire-Marcel 2010; Dipre *et al.* 2018; Geibert *et al.* 2021) led to considering a drastically distinct time frame for the Arctic Ocean events beyond the radiocarbon time scale (see Hillaire-Marcel & de Vernal 2022). Therefore, the question about the resilience or recurrence of the ESIS during the glaciations after the Mid-Pleistocene Transition is still open.

In the present study, we intend to document further the ESIS history, mostly based on the study of a core raised from the southernmost Mendeleev Ridge (Arc7-E25; hereafter referred to as E25). Its location at the northern edge of the ESIS, slightly below ice-scouring features, was seen as suitable for this purpose. This core was analysed by Zhao *et al.* (2022) who used the Mn-cyclostratigraphy with ages constrained based on a palaeomagnetic inclination reversal/excursion at ~285 cm interpreted as the Biwa II event, thus leading to the assignment of the base of the core to MIS 7 (Jakobsson *et al.* 2000). However, the interpretation of the palaeomagnetic inclination reversal/excursion stratigraphy in the Arctic Ocean is under discussion (e.g. Liu *et al.* 2019; Dong *et al.* 2022) and the chronological assignments of Zhao *et al.* (2022) are subject to debate. Herein, we revised the chronostratigraphy of core E25 mainly based on uranium (U)-series measurements and, for the lower part of the core, on the tentative assignment of the inclination reversal at the core bottom to the Brunhes/Matuyama boundary. Whenever needed, we complemented the existing sedimentological, mineralogical, and geochemical data with new measurements. Our key objectives were (i) to outline the history of the ESIS, within the frame of the thorium-230 excess ($^{230}Th_{xs}$)-based stratigraphy, with special attention paid to its age and duration, (ii) to document the palaeoceanography at the southern tip of Mendeleev Ridge, and (iii) to identify remote sedimentary signals from the northwestern LIS.

Background setting

The shallow continental shelves of the Arctic Ocean represent more than 50% of its total area (Jakobsson *et al.* 2003; Fig. 1). The shelves act as a major source of dissolved elements (e.g. Mn, Fe) and detrital particles for the deeper central Arctic Ocean (Macdonald & Gobeil 2012; Rogalla *et al.* 2022). Under high sea levels, i.e. during interglacials and/or interstadials, the shelves are submerged; coastal erosion and tidal and wind mixing result in the upload of particles by seasonal sea ice (Charette *et al.* 2020). Sediments are then redistributed by currents and slope processes, and through sea-ice rafting deposition along the Transpolar Drift (TPD) and Beaufort Gyre (BG) routes (Fig. 1). During glacials, marked by low sea levels and glaciated shelves, streaming pulses from surrounding ice sheets released iceberg fleets, dispersing ice-rafted debris (IRD) with a high content in sand and coarser fractions (see Polyak *et al.* 2010) as far as the Nordic seas (Dowdeswell *et al.* 1999). In comparison, IRD transported by sea ice is generally composed of finer detrital particles, with a smaller fraction of sand (see Polyak *et al.* 2010). Lastly, during deglaciations, major drainage events of glacial lakes in the northwestern LIS sector (e.g. Not & Hillaire-Marcel 2012) result in sedimentary pulses of deposition of fine dolomite-rich detrital material (Vogt 1997) throughout most of the Arctic Ocean (e.g. Hanslik *et al.* 2013), often referred to as 'PW layers' in the literature (cf. Polyak & Jakobsson 2011).

During glacial periods, two major ice sheets directly influenced the Arctic Ocean: the Eurasian Ice Sheet, and the LIS on the North American side (Stein *et al.* 2017). A hypothesized ESIS was thought to be present over the East Siberian Shelf–Chukchi Sea Borderland (Colleoni *et al.* 2016). Unlike the relatively well-known Eurasian and Laurentide ice sheets, the formation of the ESIS anchored over the East Siberian margin is far from clear. It could have resulted from the extension of the Eurasian Ice Sheet (Gasson *et al.* 2018) or of the Beringia ice cap (Colleoni *et al.* 2016), or from ice stream feedings by the LIS (Engels *et al.* 2008; Jakobsson *et al.* 2008). Recently, a glacially scoured trough discovered on the outer continental shelf of the East Siberian Sea (O'Regan *et al.* 2017) and the absence of large Late Pleistocene ice masses in northeastern Siberia (Nørgaard *et al.* 2023) make the first assumption more likely. However, the presence of a local ice cap, a Eurasian Ice Sheet extension,

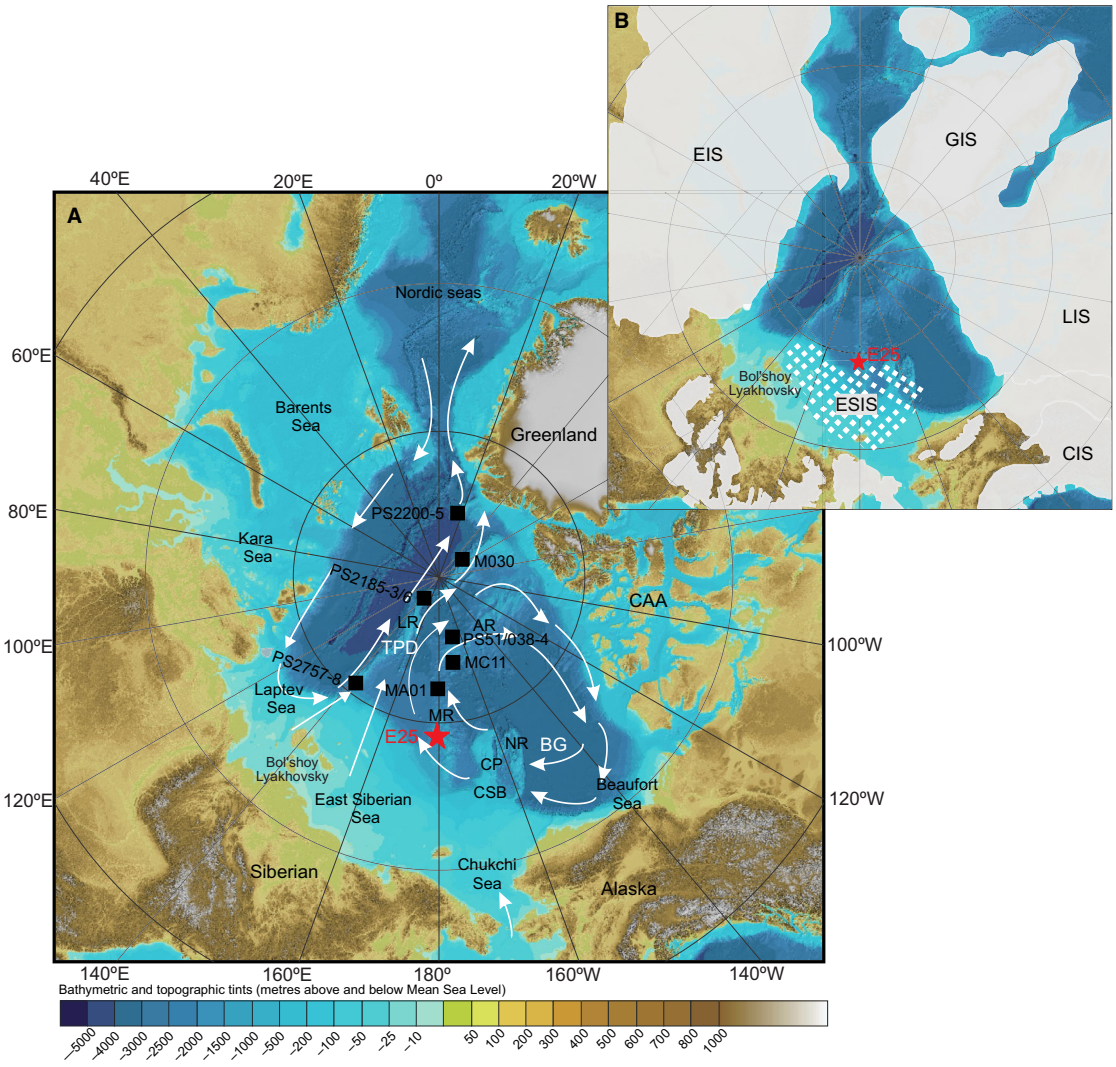

Fig. 1. Bathymetric map of the Arctic Ocean. A. Ocean circulation and site location. The white arrows = surface circulation paths; red star = the location of the study core E25; black squares = other sites mentioned in the text (from Vogt 1997; Strobl 1998; Behrends *et al.* 1999; Not & Hillaire-Marcel 2010; Hillaire-Marcel *et al.* 2017; Geibert *et al.* 2021; Xu *et al.* 2021; Purcell *et al.* 2022). B. The ice sheet/ice shelf extents. The shadow area represents the maximum ice sheet-covered areas during glaciations, as simulated by Batchelor *et al.* (2019). The red star = location of core E25. AR = Alpha Ridge; BG = Beaufort Gyre; CAA = Canadian Arctic Archipelago; CIS = Cordilleran Ice Sheet; CP = Chukchi Plateau; CSB = Chukchi Sea Borderland; EIS = Eurasian Ice Sheet; ESIS = the hypothesized location of the East Siberian Ice Shelf/Ice Sheet; GIS = Greenland Ice Sheet; LIS = Laurentide Ice Sheet; LR = Lomonosov Ridge; MR = Mendeleev Ridge; NR = Northwind Ridge; TPD = Transpolar Drift.

or a very thick ice shelf (Grosswald & Hughes 1999; Colleoni *et al.* 2016; Gasson *et al.* 2018) cannot be deciphered based on the core collected above a water depth of ~1 km, which is the depth from where ice-scouring traces were documented (e.g. Polyak *et al.* 2001; Niessen *et al.* 2013; Dove *et al.* 2014; Kim *et al.* 2021). Besides, in respect of the fact that our study core is located at the northern tip of the hypothesized ESIS, where ice thickness was only ~200 m during MIS 6 according to model simulations (Colleoni *et al.* 2016), we will thus refer to the presence of an ESIS complex, likely an ice shelf, when evidence for perennial and thick ice cover is found at the area of the studied site.

Material and methods

Material

Gravity core E25 (latitude 78°57′33″N, longitude 179°26′11″W; water depth of ~1200 m) was retrieved from the southernmost Mendeleev Ridge during the 7th cruise of the Chinese Arctic expedition on the RV 'Xue Long' in 2016. After splitting into two sections, no obvious unconformity was observed in the 320-cm-long core (Zhao *et al.* 2022). The core was continuously subsampled at 1-cm intervals and analysed for colour reflectance, dry bulk density, XRF element content,

coarse sediment fraction (>63 μm), planktonic foraminifera abundance (>154 μm), and their stable isotopic composition ($\delta^{18}O$), palaeomagnetic inclination, and mineralogy, at the First Institute of Oceanography (FIO), MNR, China and other laboratories mentioned in Zhao *et al*. (2022).

As $^{230}Th_{xs}$ records cannot provide any robust stratigraphy beyond the last four climatic cycles due to its decay within this time frame, complementary measurements were undertaken at Geotop-UQAM, initially down to 163 cm, i.e. at the depth expected to reach MIS 11 based on our initial stratigraphical estimate from FIO data. To assess any potential surface sediment loss, ^{210}Pb and ^{226}Ra measurements were performed in the upper 10 cm of the core. Below, subsampling at variable intervals ranging from 2 to 16 cm was carried out to obtain a better resolution for critical intervals. Our initial data sets were obtained from the sampling interval of 0–163 cm for U-Th series measurements. The Mn/Al ratio, planktonic foraminifera (>154 μm) abundance, and three AMS ^{14}C dates are from Zhao *et al*. (2022). In addition, AMS ^{14}C measurements on a fish otolith recovered from the surface sample (0–1 cm), and on a planktonic foraminifera assemblage between 2 and 3 cm were conducted at the Alfred Wegener Institute (Bremerhaven, Germany), and the Andre E. Lalonde AMS Laboratory of the University of Ottawa (Ottawa, Canada), respectively. They yielded conventional ^{14}C ages of ~3.28±0.08 and ~6.58±0.03 ka, respectively. Contrary to Zhao *et al*. (2022), we only used the top five ^{14}C ages to estimate recent (MIS 1 to MIS 3) sedimentation rates, as ^{14}C activities in foraminifera shells from deep-sea sediments are not reliable beyond ~35 ka (e.g. Broecker *et al*. 2006; Haynert *et al*. 2011). Examples of ^{14}C-chronological inversions in Arctic Ocean cores can be found in many papers (e.g. Clark *et al*. 1986; Darby *et al*. 1997; Adler *et al*. 2009). See Hillaire-Marcel *et al*. (2022b) for a deeper examination of ^{14}C-based chronologies in low sedimentation rate sites of the Arctic Ocean.

Methods

All methods described below refer to measurements performed at Geotop-UQAM. The methods used for measurements by Zhao *et al*. (2022) are described in the original paper.

Grain-size analysis. – A total of 36 subsamples of ~0.3 g each subsampled at intervals of 2–20 cm in the upper 167 cm of the core were selected to conduct the grain size measurement using laser-diffraction equipment. The uneven sampling depths are due to insufficient sample quantity for the grain-size measurements. Below 167 cm, the grain-size measurements were taken at 4-cm intervals. The subsamples were treated with 30% H_2O_2 and 3% HCl to remove organic matter and calcite, in particular foraminifera shells. After drying and rinsing, Na-hexametaphosphate was then added to disperse the sediments for more than 24 h. Subsamples were treated in an ultrasound bath for 30 s, followed by rotated agitation. The disaggregated sediment samples were then analysed with a laser-diffraction particle-size analyser (LS13320; Beckman-Coulter™) for the fractions smaller than 2000 μm. The grain size data and granulometric statistics were processed using GRADISTAT software (Blott & Pye 2001). The analytical reproducibility is better than 1%, according to Daubois *et al*. (2015).

X-ray diffraction measurement. – About 0.2 g of ground bulk sediments was used for X-ray diffraction measurement with a Siemens D-5000™ diffractometer (CoKα 1, 2 radiation and a silicon detector). Semi-quantitative estimates of the main mineral species were based on their main diffraction peak height (in counts per second) with automatically applied correction factors using the Bruker DIFFRAC-EVA™ software. The percentage of each mineral was estimated from its relative peak height corrected for quartz and normalized to 100%. Analytical errors are estimated to be below 5% (Not & Hillaire-Marcel 2010).

Organic carbon and $^{13}C_{org}$ measurements. – Bulk sediments were dried in the oven at ~50 °C for more than 24 h. Two aliquots of ~15 mg dry ground subsamples were acidified with concentrated HCl for more than 24 h to make sure that any detrital dolomite was totally removed. The organic carbon (C_{org}) and $^{13}C_{org}$ measurements were performed using a Carlo Erba™ elemental analyser and an Isoprime-100™ mass spectrometer, respectively. The results of $^{13}C_{org}$ measurements are expressed using the standard δ notation in comparison with the Vienna Pee Dee Belemnite (VPDB). The analytical precision is estimated at ±0.05% for C_{org} and better than ±0.1‰ for $\delta^{13}C_{org}$ based on replicate analyses of the study samples.

U-series isotopes. – Lead-210 (^{210}Pb): About 0.2 g-aliquots of the core top samples was dried and ground for ^{210}Pb measurement at 1-cm intervals, excluding between 6 and 8 cm (samples lost). Details related to the ^{210}Pb extraction and analysis can be found in Song *et al*. (2022). The standard deviation from alpha counting statistics averages 3% of the value obtained.

Radium-226 (^{226}Ra): ^{226}Ra activity was measured by gamma-ray using an EGG-Ortec gamma well detector (pure germanium) spectrometer. Pre-weighed sediment samples were sealed in 10-cm^3 glass vials for at least 21 days to ensure the secular equilibrium between ^{226}Ra and ^{222}Rn. Only five samples of the top 10 cm were large enough to allow for ^{226}Ra measurements. The ^{226}Ra-activities were determined from the measurement of the daughter ^{214}Pb (295.2, and 351.9 keV) and ^{214}Bi (609.3 keV) decay products. Counting continued until reaching an uncertainty of less than 10%.

U-Th series: Analyses of ^{230}Th, ^{234}U and ^{238}U were performed on dried and ground bulk sediment samples (~0.15 g). Powdered samples were spiked using a mixed ^{233}U-^{236}U-^{229}Th solution of known ratios and dissolved by a series of concentrated acids (HF-HNO_3-HCl-H_3BO_4). Digested samples were loaded onto AG® 1-X8 anionic exchange resin for U-Th separation. Th and U were further purified through AG® 1-X8 and UTEVA® resins, respectively. Both Th and U fractions were then analysed on a Nu Plasma™ multi-collector inductively coupled plasma mass spectrometer (MC-ICP-MS) by peak jumping on a filtered ion counter. Mass bias was corrected by the exponential law using the ^{236}U/^{233}U ratio. All results were quoted at ±2σ standard deviation uncertainty level. The HU-1 solution was used as a standard solution to monitor analytical sessions. Duplicated analyses of the HU-1 solution yielded a mean activity ratio of ^{234}U vs. ^{238}U of 1.0022±0.0049 (±1σ; n = 7). For the present study, estimates of the excess in ^{230}Th ($^{230}Th_{xs}$) activity were obtained from the equation: $A^{230}Th_{xs} = A^{230}Th - A^{234}U_{mean}$, where A is the activity in disintegrations per minute and per gram (dpm g^{-1}). Details about the calculation of $^{230}Th_{xs}$ can be found in Purcell *et al.* (2022) and the discussion below.

Analytical data are reported with one standard deviation except for U and Th isotope data which are reported with two standard deviations. All mean estimates are reported with one standard deviation.

Results

Sedimentological properties

Laser-based grain-size measurements indicate that core E25 is mostly composed of silty clay, with some intervals containing up to ~14.2 dry weight per cent (dw%) of sand (Fig. 2). The bottom layer, from 55 to 167 cm, shows a low sand content (1.7±2.5 dw%), low mean grain size (Φ) values (6.2±2.8 μm), and a high clay fraction content (33.5±4.7 dw%). The intermediate layer, from 38 to 55 cm, depicts much higher sand content (7.1±5.1 dw%) and higher Φ-values (15.8±5.8 μm), but a lower clay content (20.7±3.2 dw%). The upper layer is characterized by a low sand content (0.6±0.9 dw%), low Φ-values (6.0±2.4 μm), and an intermediate clay content (29.5±6.7 dw%).

Major mineralogical features

Mineralogical data from bulk sediments indicate that quartz (45±4%), albite (18±3%), and illite (12±2%) are the three dominant minerals. Dolomite shows peaking values from ~118 to 94 cm (up to ~9%) and from ~34 to 18 cm (up to ~13%) and does not show any significant relationships with the sand content, thus suggesting distinct depositional mechanisms. Three major calcite peaks are observed. They correlate with the foraminifer abundance (R^2 = 0.59; see Fig. S1). In these intervals, the calcite/dolomite ratio averages 2.9±0.8 vs. 1.7±0.4 in other intervals. Smectite, which is often used as a tracer of the Laptev Sea and/or the Bering Sea sediment sources (Wahsner *et al.* 1999; Viscosi-Shirley *et al.* 2003; Song *et al.* 2022), records low abundance. It does not exceed 0.5% in the upper 115 cm and rises to ~1.5% below 122 cm. Due to the uncertainties in semi-quantitative estimates of clay minerals through bulk X-ray mineralogy measurement, this difference must be interpreted with caution.

Organic carbon content and its isotopic composition

The C_{org} content in core E25 is very low, less than 0.33 dw%. It shows an overall decreasing trend downcore (Fig. 2). From the core top to 29 cm, it averages 0.29±0.02 dw% with two excursions toward lower values, notably one at ~9 cm, where it falls below 0.09 dw%. Deeper downcore, down to ~71 cm, it averages 0.19±0.02%. Below, from 71 to 163 cm, it averages 0.07±0.02 dw%.

$\delta^{13}C_{org}$ values vary from −25.3 to −22.3‰. A similar range was reported for the Chukchi Sea Rise (Park *et al.* 2017). From the core top to ~71 cm, the mean $\delta^{13}C_{org}$ value is −23.2±0.5‰. Below, it decreases to −24.3±0.9‰. Worthy of mention is the fact that the upper two samples from the core top record the maximum $\delta^{13}C_{org}$ values (~ −22.4‰), pointing to a prominent contribution of marine carbon (Schubert & Calvert 2001). Downcore, slight oscillations toward higher $\delta^{13}C_{org}$ values characterize several intervals. They may similarly relate to enhanced marine carbon supplies.

Radiocarbon ages

The radiocarbon ages range from ~3.3 to ~34.5 ka from the core top to 26 cm (Fig. 2; Table 1). However, such ages should be used with caution as mixing by benthic fauna may result in smoothing. This is particularly critical at sites characterized by low sedimentation rates (e.g. Adler *et al.* 2009), where the mixing of Holocene and pre-LGM populations may occur (Hillaire-Marcel *et al.* 2022b).

U-series isotopes

There is no measurable excess in ^{210}Pb ($^{210}Pb_{xs}$) at the core top vs. its parent ^{226}Ra isotope (see Table S1). Most Arctic Ocean sites show some $^{210}Pb_{xs}$ at the sediment surface, even those with very low sedimentation rates (i.e. <1 cm ka^{-1}; e.g. Not *et al.* 2008; Not & Hillaire-Marcel 2010). However, some other sites, notably from the Lomonosov Ridge, seem also deprived of any $^{210}Pb_{xs}$

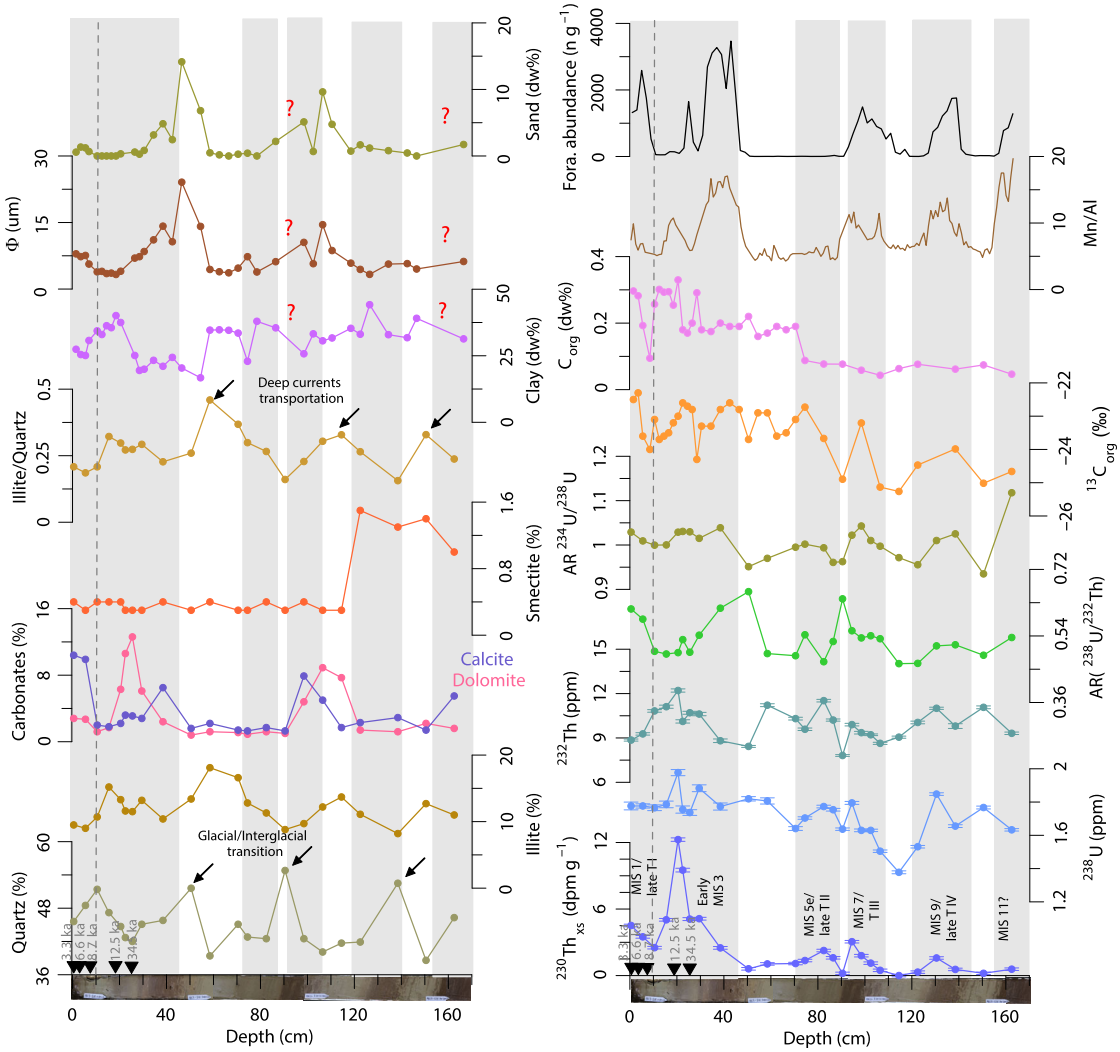

Fig. 2. Major sedimentological, mineralogical (left), and geochemical (right) features of the 0 to ~167 cm section of core E25 (see Tables S2–S4 for details). The dashed dark grey lines correspond to the Last Glacial Maximum (LGM) sedimentary gap (see text); light grey shadows highlight layers assigned to early/middle interglacial/interstadial (odd MIS numbers) or late Termination (T) intervals; red question marks point to intervals of insufficient sedimentological data. Photographs of the studied core section, Mn/Al ratio and foraminifer abundance are from Zhao *et al.* (2022); all other measurements are from the present study.

at the very surface of the sediment (e.g. PS87/023-2; Le Duc 2018).

The ^{238}U and ^{232}Th contents vary between 1.38–1.98 ppm and 7.81–12.21 ppm, respectively (Fig. 2). The AR(^{238}U/^{232}Th) value averages 0.53±0.05, a value in the lower range of those reported elsewhere in the Arctic Ocean (e.g. Not & Hillaire-Marcel 2010; Gusev *et al.* 2013; Hillaire-Marcel *et al.* 2017). The AR (^{234}U/^{238}U) has a mean value of 1.00±0.04, suggesting a near-secular equilibrium between these two isotopes. A

Table 1. Radiocarbon ages of core E25. The ^{14}C ages are uncalibrated as they are in part mixed between populations of distinct ages (see Hillaire-Marcel, *et al.* 2022b).

Interval (cm)	Depth (cm)	Material	Conventional age (year)	Error (±2σ)	Source
0–1	0.5	Fish otolith	3277	76	This study
2–3	2.5	Planktonic foraminifer	6578	29	This study
6–8	7.0	Planktonic foraminifer	8670	30	Zhao *et al.* (2022)
18–20	19.0	Planktonic foraminifer	12540	40	Zhao *et al.* (2022)
24–26	25.0	Planktonic foraminifer	34500	260	Zhao *et al.* (2022)

high AR(^{234}U/^{238}U) value (~1.12) is observed at the interval of 162–163 cm, which may relate to the U relocation driven by late diagenetic processes (Purcell *et al.* 2022), but as it concerns an insignificant U concentration change, its impact on the ^{230}Th$_{xs}$ estimate should remain within error bars.

The ^{230}Th$_{xs}$ profile of core E25 follows closely those reported for most Arctic Ocean sites (Not & Hillaire-Marcel 2010; Hillaire-Marcel *et al.* 2017; Geibert *et al.* 2021). Peaking ^{230}Th$_{xs}$ values were thus assigned to specific marine isotope stages (MIS 1, 3, 5e, 7, 9, 11) and their corresponding Ts, as shown in Fig. 2.

Discussion

The ^{230}Th$_{xs}$-based chronostratigraphy of core E25

U-Th series isotopes in core E25. – All parameters that could affect a reliable estimate of ^{230}Th$_{xs}$, i.e. of the ^{230}Th-fraction strictly inherited from the ^{230}Th produced in the water column and accumulated in sediments through scavenging processes, were summarized by Purcell *et al.* (2022). These parameters include (i) any potential marine U-uptake in surface sediments, (ii) any late diagenetic U-mobility driven by redox gradients in the sedimentary column. In both cases, the C_{org} concentration is critical for the development of low Eh horizons driving U-precipitation, either from the water column or from detrital minerals of over/underlying oxidized layers in the U^{4+} state, with preferential uptake of ^{234}U in the case of diagenetic processes (Gariépy *et al.* 1994; McManus *et al.* 2005; Wall & Krumholz 2006; Purcell *et al.* 2022).

Here, core E25 is featured in low C_{org} content and oxidizing conditions, unlikely to result in early or late diagenetic U uptake. If any, U losses from the sedimentary column toward the water column should have been modest as indicated by the near secular equilibrium between ^{230}Th and ^{234}U in layers deprived of any ^{230}Th$_{xs}$.

Similarly, any significant enrichment in ^{234}U (vs. ^{238}U) can be discarded as indicated by the mean δ^{234}U value observed (0±4‰). Any uptake of marine U at the water/sediment interface or any late diagenetic U-relocation downcore should result in excesses vs. deficits in ^{234}U as, in the first case, the marine U shows a δ^{234}U value of ~114‰ (e.g. Chen *et al.* 1986; Not *et al.* 2012); in the second case, even greater excesses in ^{234}U could be expected (e.g. δ^{234}U of ~149‰ in C_{org}-rich layers of Lomonosov Ridge core PS2757-8; Purcell *et al.* 2022).

At last, U concentrations in the cored sequence (mean [U] = 1.72±0.13 ppm) are much less variable than those of Th ([Th] = 9.94±1.13 ppm) and the overall variability of the ^{238}U/^{232}Th mass ratio is mostly driven by ^{232}Th variability (Fig. S2). Altogether, this suggests that the minor changes in U concentrations observed are linked to variable detrital sediment sources.

The correlations between AR(^{238}U/^{232}Th), and sedimentological and mineralogical properties indicate that the AR(^{238}U/^{232}Th) value is relatively high in intervals with enhanced IRD supplies and high quartz contents (Fig. S3). High AR(^{238}U/^{232}Th) seems to be linked either to high coastal erosion and sea-ice rafting under high sea levels (i.e. interglacials and MIS 3) or to glacial advances during stadials (cf. Purcell *et al.* 2022).

Calculation of the ^{230}Th$_{xs}$ extinction depth. – In the present study, we followed the approach of Purcell *et al.* (2022) for the calculation of the extinction depth and age of ^{230}Th vs. its parent ^{234}U. Even under the sporadic sedimentation regime of the Arctic Ocean (e.g. Hillaire-Marcel *et al.* 2017, 2022a), ^{230}Th$_{xs}$ broadly follows a negative exponential decay downcore. As illustrated in Fig. 3, the linear trend of ln(A^{230}Th) downcore illustrates an R^2 value of 0.57. Its intercept with the mean A^{234}U value yields a ^{230}Th 'extinction' age of 402±20 ka, at a depth of 166+64/−45 cm, taking into consideration the uncertainties on the slope of the ln (A^{230}Th) line and mean ^{234}U activity.

The ^{230}Th$_{xs}$-based stratigraphy. – As documented previously by Huh *et al.* (1997), ^{230}Th$_{xs}$ profiles in the Arctic Ocean depict a strong 'sub-surface' peak. It has been assigned to the early MIS 3, based on sequences with sedimentation rates high enough to decipher the MIS 3 peak from that of MIS 1 (see Hillaire-Marcel *et al.* 2017; Purcell *et al.* 2022). These two peaks sometimes overlap at sites with very low sediment accumulation, often characterized by an MIS 2 hiatus (Fig. 4; Not & Hillaire-Marcel 2010; Hillaire-Marcel *et al.* 2017). So far, there is no well-documented explanation for the peaking ^{230}Th$_{xs}$ values of MIS 3. Hillaire-Marcel *et al.* (2022a) proposed

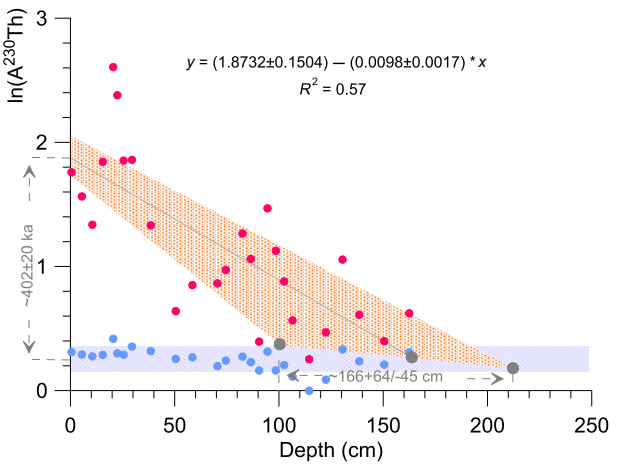

Fig. 3. Linear correlation of ln(A^{230}Th) value vs. core depth. Blue dots = ln(A^{234}U); light blue area = the uncertainty envelopes are ±1σ; red dots = ln(A^{230}Th). The intercept of ln(A^{230}Th) vs. ln(A^{234}U) corresponds to a ^{230}Th$_{xs}$ extinction age of 402±20 ka, reached at a depth of 166+64/−45 cm.

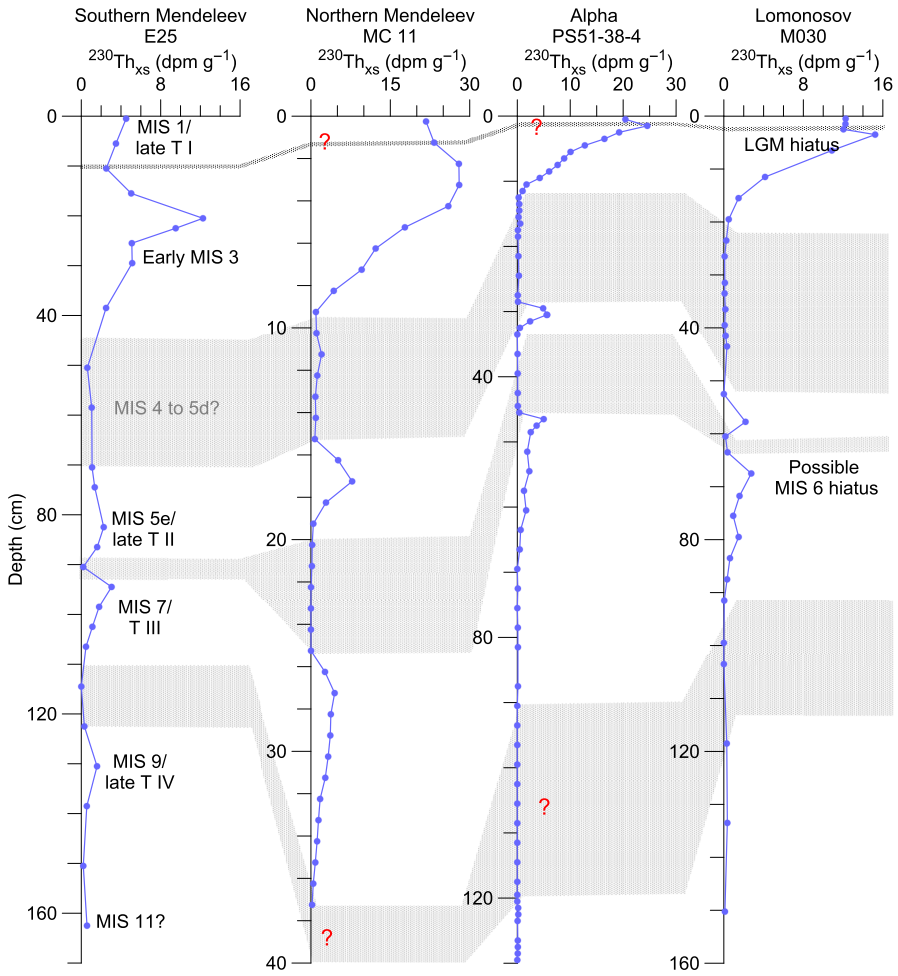

Fig. 4. $^{230}Th_{xs}$ distributions in a few sites from the Arctic Ocean ridges. The grey shadow area = sedimentations during glacials, including the LGM and possible MIS 6 hiatuses; red question marks = equivocal depth of LGM hiatus and interval of MIS 8. The raw U-Th series data are from the present study (E25), Not & Hillaire-Marcel (2010) for MC11, Hillaire-Marcel *et al.* (2017) for M030, and Geibert *et al.* (2021) for PS51/038-4.

that this $^{230}Th_{xs}$ peak results from its build-up in the water column during the preceding MIS 5d–4 interval, followed by its rapid scavenging during the early MIS 3 sea level rise (e.g. Siddall *et al.* 2008). The high MIS 3 sea level likely led to the opening of the Bering Strait (Farmer *et al.* 2023) and the submergence of the Arctic Ocean shelves, possibly accompanied by seasonal sea-ice openings and sea-ice rafting deposition of $^{230}Th_{xs}$ scavenging compounds (organic matter and clays; cf. Purcell *et al.* 2022). Note that Geibert *et al.* (2022) associated the high $^{230}Th_{xs}$ values of samples in the MIS 3 interval with continuous but low sedimentary fluxes, considering that 'even a short particle pulse would be enough to remove ^{230}Th from the water column'.

Below the MIS 3 $^{230}Th_{xs}$ peak, two intervals with measurable peaking $^{230}Th_{xs}$ values are identified. They are usually assigned to the MIS 5 and 7 and their corresponding Ts (TII, TIII; Not & Hillaire-Marcel 2010; Hillaire-Marcel *et al.* 2017; Purcell *et al.* 2022). As documented by Geibert *et al.* (2021), reduced $^{230}Th_{xs}$ values mark the MIS 4 and MIS 6, possibly pointing to very low sediment accumulation rates, and even to a sedimentary hiatus in some areas of the central Arctic Ocean during MIS 6 (Fig. 4), not unlike those of MIS 2 (see also Hillaire-Marcel *et al.* 2017). Regardless of the consensus about the assignment to MIS 6, the identification of the MIS 4 layer is still under debate. Purcell *et al.* (2022) suggested that the low $^{230}Th_{xs}$ interval between the last interglacial (MIS 5e) and MIS 3 $^{230}Th_{xs}$ peaking layers should be assigned to MIS 5d–4 considering the overall low summer season insolation and sea level conditions during this period (Hillaire-Marcel *et al.* 2021). As shown in Fig. 4, $^{230}Th_{xs}$ peaks during MIS 5a and 5c could not be recognized, leading us to adopt the advanced stratigraphy proposed by Purcell *et al.* (2022) for this study.

Following Not & Hillaire-Marcel (2010) and Purcell *et al.* (2022), the two lower minor peaks of measurable excesses in ^{230}Th illustrated in Fig. 4 could be assigned to MIS 9 (~120 to 145 cm) and 11 (~163 cm). This

stratigraphy would support the assignment of the major long-duration magnetic reversal observed at a depth of ~285 cm (Zhao *et al*. 2022) to the Brunhes/Matuyama boundary (~780 ka; deMenocal *et al*. 1990), thus fitting with the magnetostratigraphy proposed in early papers (e.g. Herman 1970; Clark *et al*. 1980; Aksu & Mudie 1985), and supporting the concept of a 'sediment starved' glacial Arctic Ocean.

Sedimentary regimes

Sedimentological features: sea-ice vs. iceberg rafting. – Coarse particles in the sediments are often used to track the ice-rafting events in the Arctic Ocean (Polyak *et al*. 2010), as they are delivered by either sea ice or icebergs. To recognize these two distinct transport processes from grain-size measurements, several approaches have been applied (Lisitzin 2002). For example, Spielhagen *et al*. (2004) proposed that icebergs were the predominant carrier of particles larger than 63 μm, whereas Dowdeswell *et al*. (1999) considered the fractions larger than 250 μm as being transported by icebergs. Adler *et al*. (2009) and Polyak *et al*. (2009) considered that larger than 63 μm fractions were compatible with sea-ice rafting. However, sea ice anchored over the continental shelf could entrain all particle-size materials and transport them toward the deep sea (Reimnitz *et al*. 1987). Later on, Polyak *et al*. (2010) suggested that sediments with a high sand content, larger than 10–20 dw%, were more likely transported by icebergs, whereas sediments with less than 5–10 dw% of sands were rather delivered by sea ice. In addition, dry weight data should be used with care as one single gravel- or pebble-sized particle could significantly bias the content of coarse fractions. At last, other processes, such as current winnowing, turbidity, etc., could also affect the grain-size distribution (see Stein 2008).

In core E25, the sand content is low, varying between 0 and ~14 dw% with a median below 2 dw%. In opposition, the clay content varies between ~17 to ~44 dw% with a median of about 31 dw%. These data point to the unlikeness of any long-duration IRD deposition by icebergs except possibly for the ~14 and ~10 dw% peaking sand contents at ~50 and ~105 cm, respectively. The corresponding intervals could be assigned here to the late MIS 4 and MIS 8 glacial stages. However, the grain size data fit better with sea ice or deep current transport mechanisms throughout most of the recorded interval of core E25, except for the MIS 4/3 transition. Indeed, grain-size measurements in 'dirty' seasonal sea ice and shelf sediments from the Laptev Sea by Dethleff (2005) depict a distribution similar to that generally characterizing core E25 (~30 dw% of clay; ~63 dw% of silt; ~7 dw% of sand). Worthy of mention here is the fact that ^{14}C ages of surface sediments from sites that are presently covered by perennial sea ice vary from ~8 to 5 ka (e.g. Spielhagen *et al*. 2004; Not & Hillaire-Marcel 2010; Hillaire-Marcel *et al*. 2017; de Vernal *et al*. 2020; Xiao *et al*. 2020), implying very little sedimentation in the central Arctic Ocean under perennial sea ice, which is almost sediment free.

During glacial intervals, with the development of ice shelves (e.g. Dowdeswell & Jeffries 2017), sedimentation was mostly linked to meltwater plumes (e.g. Reilly *et al*. 2016), resulting in a high content of fine silt-clay particles (<11 μm; ~82 dw%) and almost nil sand deposition (~1 dw%; cf. Jennings *et al*. 2022).

Whenever ice advance or retreat occurred, sporadic coarse particle deposition by icebergs would be expected. According to Clark & Hanson (1983), it should be characterized by low clay (~7 dw%) and high sand (up to 27 dw%) contents. On these grounds, using both coarse and fine fractions seems an appropriate means to assess the ice-rafting transport process. The Φ-value, whose variation has been associated with the coarse fraction content (e.g. Not & Hillaire-Marcel 2010), can additionally be used to reflect ice condition changes in the Arctic Ocean.

As illustrated in Fig. 2, two intervals depict Φ-values >10: the MIS 8/7 and MIS 4/3 transitions, the latter being the most important. The Φ-values may suggest some ice streaming or open sea-ice conditions, possibly related to the dislocation of the ESIS (Dove *et al*. 2014; O'Regan *et al*. 2017; Schreck *et al*. 2018; Kim *et al*. 2021). With the exception of the above intervals marked by coarser sediment, the interval encompassing the MIS 11 to MIS 4/3 transition is characterized by low sand (0.7±0.5 dw%), high clay (34.4±4.7 dw%) and fine silt-clay (84.8±5.6 dw%) contents, and a low Φ-value (5.0±1.1 μm), suggesting lateral transport of fine sediments, possibly through subglacial drainage systems (Jennings *et al*. 2022).

Sediment fluxes. – Sediment accumulation in the central Arctic Ocean was low during glacials, almost nil during MIS 2 (Not & Hillaire-Marcel 2010), and possibly MIS 6 (Hillaire-Marcel *et al*. 2017; Geibert *et al*. 2021). Moreover, during glacial stages or transitions, coarse sediments were deposited whenever ice retreat or ice advance occurred as suggested by Purcell *et al*. (2022). Thus, inferences about effective sedimentation rates for such sequences would be misleading.

In core E25, sediment accumulation mostly occurred during depositional windows of early/middle interglacial (or interstadial in the case of MIS 3) intervals. These accumulations cannot be assigned to a specific time-span, as they were linked to high sea-ice rafting rates and/or lateral transportation, thus to intervals with submerged shelves, and high summer insolation values (Hillaire-Marcel *et al*. 2021). For example, during the present interglacial, sedimentation resumed at ~8 ka in the central Arctic but decreased rapidly

during the Neoglacial starting at about 4 ka (e.g. Darby *et al.* 1997; Adler *et al.* 2009; de Vernal *et al.* 2020). Thus, the few cm of 'interglacial/interstadial' sediment accumulated at sites, such as the one of core E25, were deposited within a few thousand years. Nonetheless, we have tentatively outlined a stratigraphical scheme for core E25 in Fig. 5, with possible depositional time windows. Except for the interval assigned to MIS 3, the sedimentary regime would have led to an overall near-linear age-depth trend for these time windows throughout the whole record. The outlined stratigraphy based on $^{230}Th_{xs}$ distribution and decay downcore is of course different from that proposed by Zhao *et al.* (2022), mainly set from the Mn-based cyclostratigraphy and the PW layer depths, pointing to a significantly lower overall sediment accumulation during relatively short time windows in opposition to the higher sedimentation rates proposed by Zhao *et al.* (2022) (see Hillaire-Marcel & de Vernal 2022).

Terrestrial supplies during the late Quaternary

Detrital carbonate pulses from the Canadian Arctic Archipelago. – Dolomite in sediments from the Arctic Ocean represents supplies from the Canadian Arctic Archipelago (CAA) and northern Greenland, where source rocks outcrop. Dolomite is thus a tracer of ice-rafting (Bischof *et al.* 1996; Vogt 1997) and/or glacial lake drainage events (Not & Hillaire-Marcel 2012; Swärd *et al.* 2022) from the Mackenzie region. At site E25, dolomite peaks at about 13% during MIS 7/late TIII and MIS 3, when it reaches up to ~40% at two sites from the northern Mendeleev Ridge investigated by Not & Hillaire-Marcel (2010), about 250 nautical miles northward (Figs 1, 6). Another distinct feature of the dolomite record from core E25 is that the MIS 5e/late TII pulse is missing whereas the northernmost Mendeleev sites recorded systematically such pulses for all deglaciations including the MIS 5e/late TII interval (Fig. 6; Not & Hillaire-Marcel 2010). The sheltered situation of coring site E25 and/or its isolation from the western Arctic Ocean margin due to the existence of the ESIS (Ye *et al.* 2020), could explain these discrepancies. However, the fact that sites from the central Lomonosov Ridge and the Morris Jesup Rise (PS2185-3/6 and PS2200-5; Fig. 6), as well as Amerasian Basin (PS72/396-3/5) and Alpha Ridge (PS51/038-4), also recorded a reduced, even negligible, dolomite pulse during MIS 5e/late TII (Geibert *et al.* 2021), suggests a weak discharge/drainage event from the northwestern LIS toward the Arctic Ocean (Dalton *et al.* 2022).

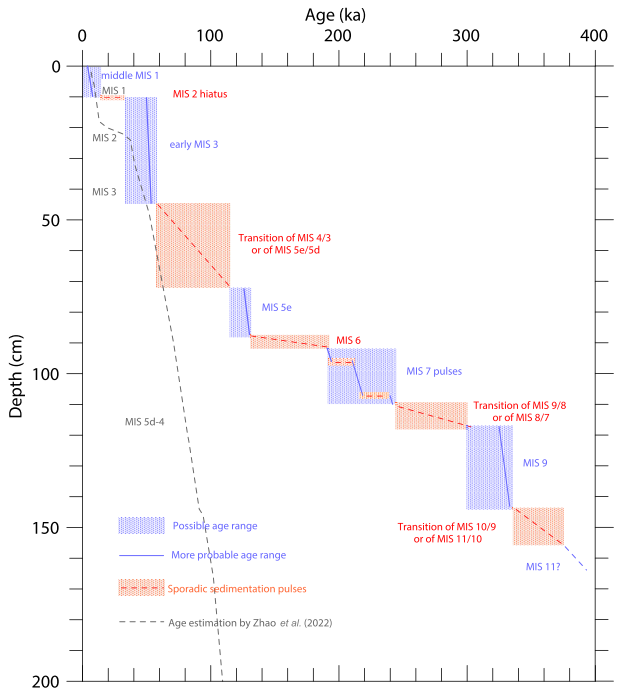

Fig. 5. Outline of a tentative chronostratigraphy in core E25 based on $^{230}Th_{xs}$ distribution. The effective duration of sedimentary pulses is open to discussion, but probable sedimentary windows are indicated by thick lines, blue for sea-ice rafting deposition during 'warm' intervals (i.e. with a high sea level/high insolation for sea-ice rafting deposition; see text), and red dashed for sediments deposited during late or early transitions. Grey dashed line: chronostratigraphy proposed by Zhao *et al.* (2022) using the Mn-based cyclostratigraphy. Shadow areas mark the maximum duration of the intervals.

The detrital carbonate layers referred to as 'PW III' and 'PW II' were tentatively assigned to MIS 3 and 5d, respectively, based on the records of stable carbon and oxygen isotopes of planktonic foraminifer and planktonic foraminifer abundances (e.g. Polyak *et al.* 2004; Spielhagen *et al.* 2004; Stein 2008). However, the 'PW II' should be re-assigned to the early MIS 7/late TIII (Fig. 6), following the present $^{230}Th_{xs}$-based stratigraphy and the chronostratigraphy proposed initially by Spielhagen *et al.* (1997). Different from Spielhagen *et al.* (1997), who assigned the three ^{10}Be peaks at the interval of ~120–200 cm of core PS2185-3/6 to MIS 7, 9 and 11, we interpret the corresponding $^{230}Th_{xs}$ peaks to MIS 7 following Hillaire-Marcel *et al.* (2021) (Fig. 6) as $^{230}Th_{xs}$ could not be detected at MIS 11, even MIS 9, layer using the low-precision alpha counting analyses.

The fine-detrital dolomite peaks of MIS 7/late TIII and early MIS 3, i.e. the so-called 'PW II' and 'PW III', observed systematically in deep Arctic Ocean sequences, likely relate to some important meltwater outbursts from the northwestern LIS (Not & Hillaire-Marcel 2012; Fagel *et al.* 2014; Dalton *et al.* 2019; Swärd *et al.* 2022). Such outbursts rarely lasted more than a few hundred years (e.g. Clarke *et al.* 2004, 2009; Kleman & Applegate 2014). The spreading of detrital dolomite over relatively thick layers (up to about 20 cm at site E25; Fig. 6) suggests mixing by physical or biological processes as illustrated by the dating of biogenic

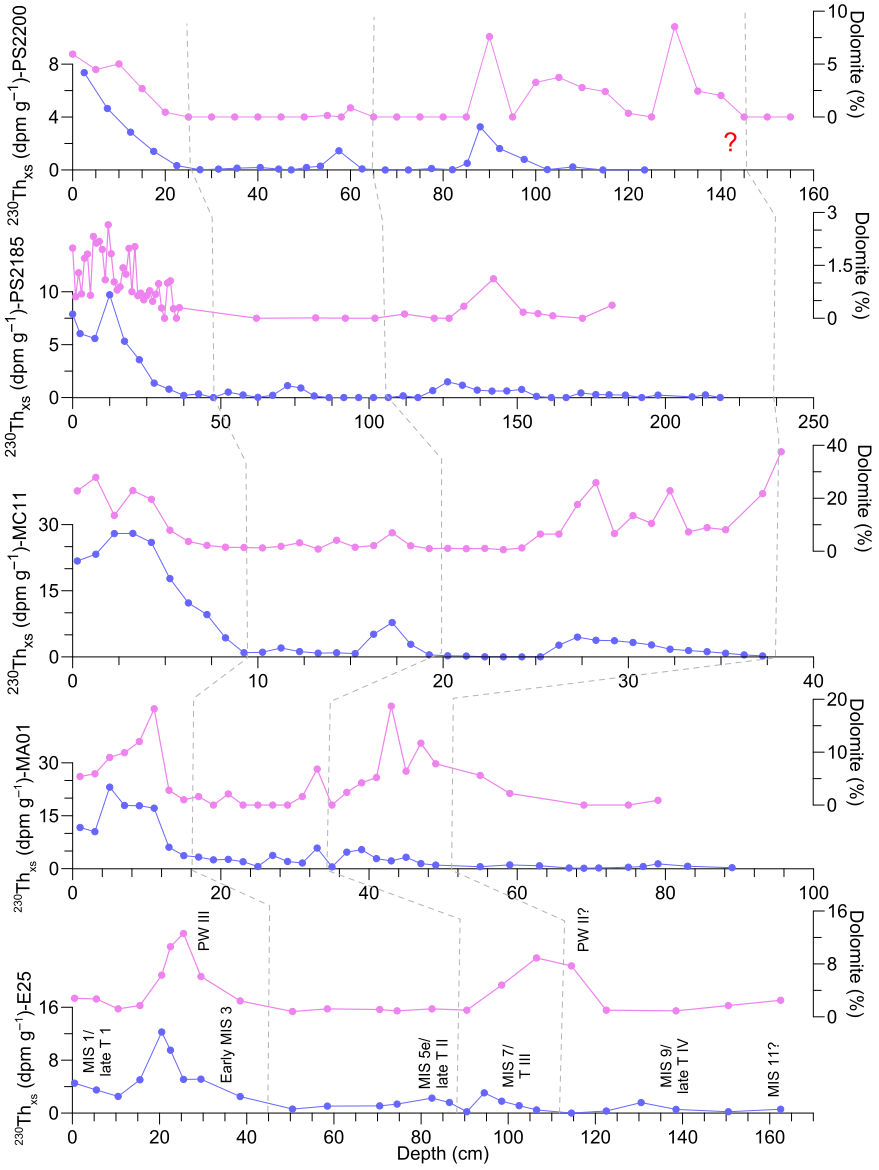

Fig. 6. Dolomite content distributions in the Arctic Ocean using the $^{230}Th_{xs}$-based chronostratigraphy. Core MA01 from Xu *et al.* (2021); core MC11 from Not & Hillaire-Marcel (2010); cores PS2185-3/6 and PS2200-5 from Vogt (1997), Strobl (1998) and Behrends *et al.* (1999). Dashed lines correspond to the inception of MIS 7/T III, 5e/late T II, and 3, respectively. The age model of core MA01 was revised here based on the $^{230}Th_{xs}$ extinction age using our method (Fig. S4). The re-interpretation of $^{230}Th_{xs}$ profiles of cores PS2185-3/6 and PS2200-5 was according to Not & Hillaire-Marcel (2010) and Geibert *et al.* (2021). The assignment of the bottom depth of the MIS 7/T III layer in core PS2200-5 was based on the ^{10}Be profile (Strobl 1998).

carbonate from low sedimentation rate sites of the Lomonosov Ridge (Hillaire-Marcel *et al.* 2022b).

Silicate supplies from the East Siberian Shelf. – Amphiboles and pyroxenes are two common heavy minerals of the East Siberian Shelf (Behrends *et al.* 1999). Their abundances in sedimentary sequences from the Lomonosov Ridge have been considered as supporting an East Siberian Ice Sheet advance hypothesis (e.g. Alatarvas *et al.* 2022). However, these two minerals are undetectable in core E25 (see also Zhao *et al.* 2022), possibly due to the overall low sand content downcore (Fig. 2). The occurrence of quartz grains has been proposed as an alternative indicator of glacial activity over the East Siberian Shelf (Bazhenova 2012; Dong *et al.* 2020). Quartz is abundant in core E25, but mostly in fine fractions. Its variations might be compatible with some deglacial pulses in the critical area (Fig. 2).

Illite, the most abundant clay mineral of the sequence, has been proposed as a primary indicator of sea-ice rafting deposition and meltwater plumes and current transportations at the Chukchi–Alaskan

margin (Ye *et al.* 2020; Koo *et al.* 2021; Wang *et al.* 2021). At site E25, the illite/quartz ratio records peak values during glacial intervals of MIS 5d–4, 8, 10 (Fig. 2), thus fitting better with deep current transportation at the site than with sea-ice rafting. As the illite/quartz ratio is proportional to illite abundance (R^2 = 0.90; Fig. S5), it seems likely that variations in illite fluxes throughout the studied interval are effective tracers of deep-current transported fine particles from the East Siberian Sea (Wang *et al.* 2021).

Resilient ice cover off the East Siberian Shelf during the late Quaternary

Several sedimentological features of core E25 can help document further the nature and resilience of the ice overlying the site during a substantial part of the recorded interval. They include (i) the relative thicknesses of sedimentary layers deposited within discontinuous time windows; (ii) the grain-size properties of the sediment; (iii) the C_{org} content; (iv) the geochemical and isotopic properties ($^{230}Th_{xs}$ in particular); (v) the microfaunal content.

In the first step, we used high clay low sand, and low C_{org} contents as major discriminants to define conditions pointing to the presence of a perennial and thick ice cover at the study site, i.e. a situation when sedimentation was mainly governed by deep currents and/or meltwater plumes beneath the ESIS, a situation when primary productivity was extremely low. Unfortunately, aside from our study core E25, only two sites (MC11 and MA01; Not & Hillaire-Marcel 2010; Xiao *et al.* 2020; Xu *et al.* 2021; Park *et al.* 2022) from the northern Mendeleev Ridge provide information about sedimentological and organic matter properties, in addition to $^{230}Th_{xs}$ profiles allowing for the set up of similar chronostratigraphies. As illustrated in Fig. 7, most core E25 data fall within the domain of perennial and thick ice, thus the resilient ESIS. The five outliers correspond to the coarse pulses we assigned to the MIS 8/7 and 4/3 transitions, with a retreating ESIS, leading to intervals with open sea-ice conditions during MIS 7 and the early MIS 3. Other northern sites from the Mendeleev Ridge area (sites MA01 and MC11), likely far from the ESIS margin (Fig. 1) and with a thinner ice cover (Colleoni *et al.* 2016), record overall coarser sedimentation and higher organic carbon fluxes linked to either iceberg-rafting events or seasonally open sea-ice conditions. Hence, a resilient ESIS cover likely prevailed in the E25 core area from MIS 11 to MIS 4, with some opening during MIS 7, while the northern sites (e.g. site MA01) show distinct features pointing to alternations of ice-streaming to sea-ice rafting events.

We should mention here that using different stratigraphical tools, distinct age models were proposed for some of the cores mentioned above (see Fig. 5). For core MA01, using the Mn-based cyclostratigraphy and the interpretation of the first palaeomagnetic inclination event to the boundary of MIS 8/7, Xiao *et al.* (2020) assigned the interval from core top to ~240 cm to the MIS 1–7 period. As this layer is characterized by a relatively high abundance of foraminifer shells, this feature was assigned to enhanced biogenic preservation under extensive sea ice cover conditions (Xiao *et al.*

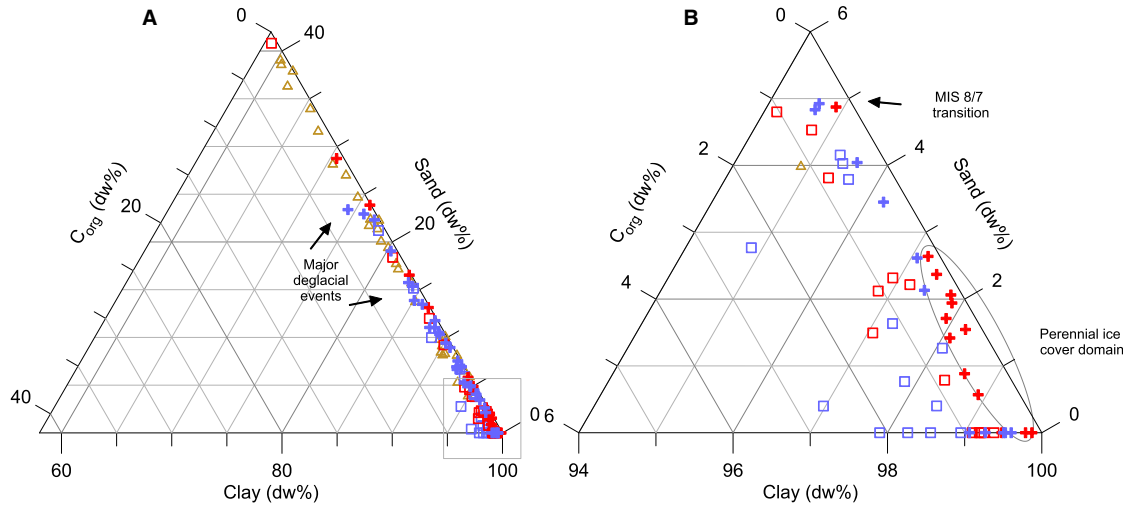

Fig. 7. Ternary analysis of clay, sand, and C_{org} contents in cores from the Mendeleev Ridge area (A) and zoom-in on the perennial ice cover cluster (B). These three components were plotted as relative percentages. Red data from the study core E25; blue data from core MA01 (Xu *et al.* 2021; Park *et al.* 2022); olive data from core MC11 (Not & Hillaire-Marcel 2010). For site E25, the perennial and thick ice cover (resilient ESIS) domain includes data from MIS 11 to MIS 4 (cross symbols), MIS 8/7 transition excluded, whereas data from the MIS 4/3 transition to the present (square symbols) and MIS 8/7 fall into the seasonal sea-ice domain. It seems that perennial and thick ice extended northward to the area of site MA01 during MIS 6 and 5d–4.

2020). Of course, based on the $^{230}Th_{xs}$ stratigraphy, the MIS 7 layer of core MA01 should be strictly assigned to the interval of 35–50 cm (Fig. 6). Within this framework, the prevalent severe ice conditions hypothesized by Xiao *et al.* (2020) should then persist for a much longer time and are not inconsistent with our findings.

Based on the stratigraphy constrained from the $^{230}Th_{xs}$ profiles, data from earlier studies of core E25 (Zhao *et al.* 2022) provide clues about conditions before MIS 11. As illustrated in Fig. 8, the resilient ESIS cover may have been initiated during the late Quaternary after the Mid-Pleistocene Transition (Bischof & Darby 1997; Dipre *et al.* 2018) following the abrupt orbital forcing changes (Tziperman & Gildor 2003), thus the low summer insolation interval that makes unlikely any major ice cover opening in the Arctic Ocean (Hillaire-Marcel *et al.* 2021).

Resilient ESIS conditions at the study site probably persisted throughout MIS 5e as there is no evidence of sea-ice rafting deposition. We hypothesize that the short duration of the high summer insolation peak of MIS 5e (Hillaire-Marcel *et al.* 2021) failed to lead to the full melt of the ESIS inherited from MIS 6 (Colleoni *et al.* 2016). The low Mn/Al ratio observed during this interval (Figs 2, 8) could relate to the presence of some ice over the East Siberian–Chukchi seas shelves, preventing the formation of Mn-oxides or their transportation toward the deep Arctic Ocean, or to complex diagenetic processes (Sundby *et al.* 2015). Furthermore, the stable isotopic composition ($\delta^{18}O$, δD) and pollen records of a layered ice/peat complex on the southern coast of the Bol'shoy Lyakhovsky Island, led Wetterich *et al.* (2016) to conclude that winter conditions during MIS 5 were colder than during MIS 3 while summer conditions

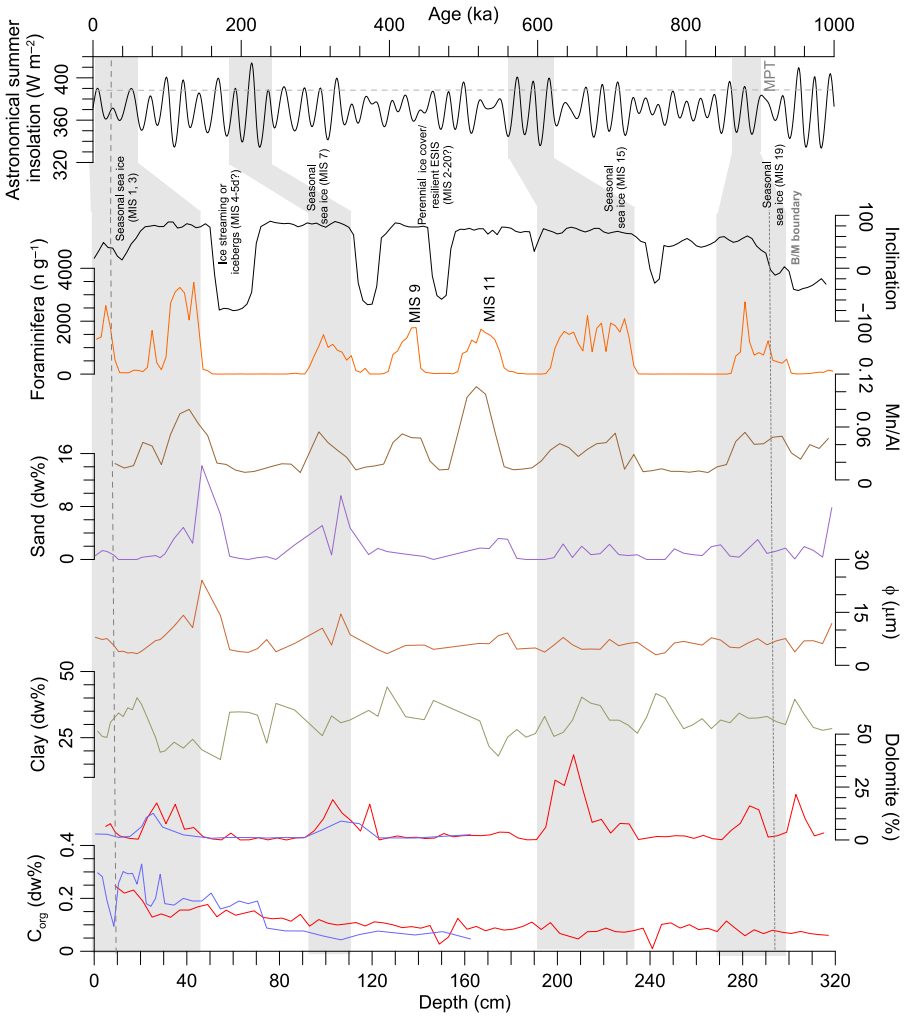

Fig. 8. Sedimentology, geochemistry, foraminifer abundance, and magnetic inclination profiles in core E25 (C_{org} in red: S. Zhao, pers. comm. 2022; other data: Zhao *et al.* 2022). Upper horizontal dashed line = mean summer insolation at the middle Holocene Thermal Maximum; left vertical dashed line = LGM hiatus; right vertical dotted line = our interpretation of the Brunhes/Matuyama reversal boundary in the core. Excursions in the Brunhes epoch are interpreted here in relation to redox-driven diagenetic processes at the edge of Mn-rich layers (see Xuan & Channell 2010; Wiers *et al.* 2020). Light grey shadowed layers correspond to interglacial/interstadials and/or late Ts likely covered by seasonal sea ice.

during MIS 5 were harsher than during MIS 3. As the Bol'shoy Lyakhovsky Island is adjacent to the postulated ESIS area (Fig. 1B), cold 'glacial' conditions over the island linked to some residual ESIS would make sense. Such cold climate conditions might have been limited to the East Siberian continental margin area, as several studies suggest summer temperatures in other areas of the Arctic Ocean are up to ~5 °C higher than at present (e.g. Miller *et al*. 2010).

Harsh conditions during MIS 5e are also suggested by the low foraminiferal abundance in the corresponding interval (less than 32 g^{-1}; Figs 2, 8), adding that these few tests might have been carried along the lower halocline from open sea-ice settings off the ESIS potential area (Zamelczyk *et al*. 2021).

During glacial stages MIS 5d–4 and earlier stadials of the Quaternary, one can hypothesize (i) a ≥800-m-thick ice shelf (Jakobsson *et al*. 2010, 2016; Geibert *et al*. 2021); (ii) an underlying freshwater layer of a few hundred metres (Hillaire-Marcel *et al*. 2022a) or possibly deeper (Geibert *et al*. 2021); (iii) a thinner but normal salinity layer below (Hillaire-Marcel *et al*. 2022a); and (iv) rare and coarse detrital fluxes linked to iceberg rafting, thus a lesser supply of fine particles (Hillaire-Marcel *et al*. 2022a). During such intervals, ^{230}Th scavenging and deposition at the sea floor were likely very low (Fig. 4; Geibert *et al*. 2021; Hillaire-Marcel *et al*. 2022a).

During the late Ts/early interglacials preceding the MIS 5d–4 cold spell and within the $^{230}Th_{xs}$ time-span (i.e. MIS 5e/TII, MIS 9/TIV, possibly MIS 11 in core E25), more significant $^{230}Th_{xs}$ scavenging and deposition occurred. However, this does not necessarily imply open sea-ice conditions in the area. Fine particle supplies by mesoscale eddies, deep currents, and down-slope nepheloid processes (e.g. Darby *et al*. 2009; Xiang & Lam 2020; Schulz *et al*. 2021; Watanabe *et al*. 2022) could have been responsible for $^{230}Th_{xs}$ advection at the study site.

Resuspended sediment could have also adsorbed Mn-oxides from the shelves, leading to the high Mn/Al ratio characterizing the early interglacial/late T transitions (Figs 2, 8). This process has already been reported in cores from the Lomonosov Ridge and Yermak Plateau, where large amounts of reworked materials rich in terrestrial organic matter, were recovered (Kremer *et al*. 2018; Purcell *et al*. 2022).

Conclusions

Using $^{230}Th_{xs}$ distribution and decay downcore, a distinct chronostratigraphy of core E25 emerges out from the earlier one which was based on the Mn-cyclostratigraphy and PW layers age assignments (cf. Zhao *et al*. 2022). It leads to inferring palaeoceanographic changes compatible with those proposed recently by Hillaire-Marcel *et al*. (2017), Geibert *et al*. (2021) and Purcell *et al*. (2022). It is also consistent with the orbitally tuned parameters governing sea-ice dynamics in the Arctic Ocean, which are the summer cumulative insolation and the sea level (Hillaire-Marcel *et al*. 2021).

As in earlier studies proposing the advance of a thick ice shelf or an ice sheet over the East Siberian Sea, our data from core E25 are in line with the presence of a resilient ice shelf extending slightly beyond the East Siberian Sea slope. Its northern tip did not extend much beyond 79.0°N (the latitude of site E25), as the northern core MA01 located at 82.0°N suggests seasonal sea-ice activity during intervals that could be assigned to interglacials or interstadials (Xiao *et al*. 2020; Xu *et al*. 2021). The inception of such a resilient ice shelf could have been linked to the MIS 14–10 low insolation interval, thus possibly marking the MIS 14 glacial inception. This thick ice seems to have been a resilient feature in the area until MIS 2 with a few episodes of ice retreat. Among those, the early MIS 3 and MIS 7, in particular, are characterized by high $^{230}Th_{xs}$ and foraminiferal counts suggesting some open ice conditions in the western Arctic. However, both tracers could have been linked to advective processes along slopes and do not ascertain the full disappearance of resilient ice over the study area.

Acknowledgements. – This work was supported by the Natural Sciences and Engineering Research Council (NSERC) of Canada, the Fonds de Recherche du Québec Nature et Technologies (FQRNT), and the National Natural Science Foundation of China (grant numbers: 41876070, 42176245). Thanks to all scientists and crews for their help with the sampling of core E25 during the 7th Chinese National Arctic Research Expeditions (CHINARE 2016). The financial support from the China Scholarship Council is highly appreciated by T. Song. Thanks to André Poirier for his kind support in the MC-ICP-MS laboratory of Geotop-UQAM. We also appreciate all technical support from Agnieszka Adamowicz, Jean-François Hélie, Julien Gogot, François Hardy, Michel Preda and Philippe Roberge. Reviews from Walter Geibert (Marum, Bremen) and Matt O'Regan (Stockholm University) helped to clarify important aspects of the manuscript. The authors declare that they have no known competing financial interests or personal relationships that could have appeared to influence the work reported in this paper.

Author contributions. – TS, CH-M and YL designed this project. TS performed all the analyses used in this study. TS and CH-M ran the statistical analyses of the obtained results. TS produced the figures and wrote the initial draft of the manuscript. CH-M, AV and YL participated in the editing and revision of the manuscript. CH-M, YL and AV acquired the funding. YL provided the samples.

Data availability statement. – All the data used in this study are available in the Supporting Information and the Pangaea database (https://doi.org/10.1594/PANGAEA.94984).

References

Adler, R. E., Polyak, L., Ortiz, J. D., Kaufman, D. S., Channell, J. E., Xuan, C., Grottoli, A. G., Sellén, E. & Crawford, K. A. 2009: Sediment record from the western Arctic Ocean with an improved late Quaternary age resolution: HOTRAX core HLY0503-8JPC, Mendeleev Ridge. *Global and Planetary Change 68*, 18–29.

Aksu, A. E. & Mudie, P. J. 1985: Magnetostratigraphy and palynology demonstrate at least 4 million years of Arctic Ocean sedimentation. *Nature 318*, 280–283.

Alatarvas, R., O'Regan, M. & Strand, K. 2022: Heavy mineral assemblages of the De Long Trough and southern Lomonosov Ridge glacigenic deposits: implications for the East Siberian Ice Sheet extent. *Climate of the Past 18*, 1867–1881.

Backman, J., Fornaciari, E. & Rio, D. 2009: Biochronology and paleoceanography of late Pleistocene and Holocene calcareous nannofossil abundances across the Arctic Basin. *Marine Micropaleontology 72*, 86–98.

Backman, J., Jakobsson, M., Løvlie, R., Polyak, L. & Febo, L. A. 2004: Is the central Arctic Ocean a sediment starved basin? *Quaternary Science Reviews 23*, 1435–1454.

Batchelor, C. L., Margold, M., Krapp, M., Murton, D. K., Dalton, A. S., Gibbard, P. L., Stokes, C. R., Murton, J. B. & Manica, A. 2019: The configuration of Northern Hemisphere ice sheets through the Quaternary. *Nature Communications 10*, 3713, https://doi.org/10.1038/s41467-019-11601-2.

Baumann, M. 1990: Coccoliths in sediments of the eastern Arctic Basin. *Geological History of the Polar Oceans: Arctic versus Antarctic 308*, 437–445.

Bazhenova, E. 2012: *Reconstruction of late Quaternary sedimentary environments at the southern Mendeleev Ridge (Arctic Ocean)*. Ph.D. thesis, Universität Bremen, 83 pp.

Behrends, M., Hoops, E. & Peregovich, B. 1999: Distribution patterns of heavy minerals in Siberian Rivers, the Laptev Sea and the eastern Arctic Ocean: an approach to identify sources, transport and pathways of terrigenous matter. *In* Kassens, H., Bauch, H. A., Dmitrenko, I., Eicken, H., Hubberten, H.-W., Melles, M., Thiede, J. & Timokhov, L. (eds.): *Land-Ocean Systems in the Siberian Arctic*, 265–286. Springer-Verlag, Berlin.

Bischof, J. & Darby, D. A. 1997: Mid-to late Pleistocene ice drift in the western Arctic Ocean: evidence for a different circulation in the past. *Science 277*, 74–78.

Bischof, J., Clark, D. L. & Vincent, J. S. 1996: Origin of ice-rafted debris: Pleistocene paleoceanography in the western Arctic Ocean. *Paleoceanography 11*, 743–756.

Blott, S. J. & Pye, K. 2001: GRADISTAT: a grain size distribution and statistics package for the analysis of unconsolidated sediments. *Earth Surface Processes and Landforms 26*, 1237–1248.

Brigham-Grette, J. 2013: A fresh look at Arctic ice sheets. *Nature Geoscience 6*, 807–808.

Broecker, W., Barker, S., Clark, E., Hajdas, I. & Bonani, G. 2006: Anomalous radiocarbon ages for foraminifera shells. *Paleoceanography 21*, PA2008, https://doi.org/10.1029/2005PA001212.

Charette, M. A., Kipp, L. E., Jensen, L. T., Dabrowski, J. S., Whitmore, L. M., Fitzsimmons, J. N., Williford, T., Ulfsbo, A., Jones, E., Bundy, R. M. & Vivancos, S. M. 2020: The transpolar drift as a source of riverine and shelf-derived trace elements to the central Arctic Ocean. *Journal of Geophysical Research: Oceans 125*, e2019JC015920, https://doi.org/10.1029/2019JC015920.

Chen, J. H., Edwards, R. L. & Wasserburg, G. J. 1986: ^{238}U, ^{234}U and ^{232}Th in seawater. *Earth and Planetary Science Letters 80*, 241–251.

Clark, D. L. & Hanson, A. 1983: Central Arctic Ocean sediment texture: a key to ice transport mechanisms. *In* Molnia, B. F. (ed.): *Glacial-Marine Sedimentation*, 301–330. Springer, Boston.

Clark, D. L., Andree, M., Broecker, W. S., Mix, A. C., Bonani, G., Hofmann, H. J., Morenzoni, E., Nessi, M., Suter, M. & Woelfli, W. 1986: Arctic Ocean chronology confirmed by accelerator ^{14}C dating. *Geophysical Research Letters 13*, 319–321.

Clark, D. L., Whitman, R. R., Morgan, K. A. & Mackey, S. D. 1980: Stratigraphy and glacial-marine sediments of the Amerasian Basin, central Arctic Ocean. *Geological Society of America, Special Paper 181*, 1–57.

Clarke, G. K. C., Bush, A. B. G. & Bush, J. W. M. 2009: Freshwater discharge, sediment transport, and modeled climate impacts of the final drainage of glacial Lake Agassiz. *Journal of Climate 22*, 2161–2180.

Clarke, G. K., Leverington, D. W., Teller, J. T. & Dyke, A. S. 2004: Paleohydraulics of the last outburst flood from glacial Lake Agassiz and the 8200BP cold event. *Quaternary Science Reviews 23*, 389–407.

Colleoni, F., Kirchner, N., Niessen, F., Quiquet, A. & Liakka, J. 2016: An East Siberian ice shelf during the late Pleistocene glaciations: numerical reconstructions. *Quaternary Science Reviews 147*, 148–163.

Dalton, A. S., Finkelstein, S. A., Forman, S. L., Barnett, P. J., Pico, T. & Mitrovica, J. X. 2019: Was the Laurentide ice sheet significantly reduced during marine isotope stage 3? *Geology 47*, 111–114.

Dalton, A. S., Stokes, C. R. & Batchelor, C. L. 2022: Evolution of the Laurentide and Innuitian ice sheets prior to the Last Glacial Maximum (115 ka to 25 ka). *Earth-Science Reviews 224*, 103875, https://doi.org/10.1016/j.earscirev.2021.103875.

Darby, D. A., Bischof, J. F. & Jones, G. A. 1997: Radiocarbon chronology of depositional regimes in the western Arctic Ocean. *Deep Sea Research Part II: Topical Studies in Oceanography 44*, 1745–1757.

Darby, D. A., Ortiz, J., Polyak, L., Lund, S., Jakobsson, M. & Woodgate, R. A. 2009: The role of currents and sea ice in both slowly deposited Central Arctic and rapidly deposited Chukchi–Alaskan margin sediments. *Global and Planetary Change 68*, 58–72.

Daubois, V., Roy, M., Veillette, J. J. & Ménard, M. 2015: The drainage of Lake Ojibway in glaciolacustrine sediments of northern Ontario and Quebec, Canada. *Boreas 44*, 305–318.

Dethleff, D. 2005: Entrainment and export of Laptev Sea ice sediments, Siberian Arctic. *Journal of Geophysical Research: Oceans 110*, C07009, https://doi.org/10.1029/2004JC002740.

Dipre, G. R., Polyak, L., Kuznetsov, A. B., Oti, E. A., Ortiz, J. D., Brachfeld, S. A., Xuan, C., Lazar, K. B. & Cook, A. E. 2018: Plio-Pleistocene sedimentary record from the Northwind Ridge: new insights into paleoclimatic evolution of the western Arctic Ocean for the last 5 Ma. *Arktos 4*, 54, https://doi.org/10.1007/s41063-018-0054-y.

Dong, L., Liu, Y., Shi, X., Polyak, L., Huang, Y., Fang, X., Liu, J., Zou, J., Wang, K., Sun, F. & Wang, X. 2017: Sedimentary record from the Canada Basin, Arctic Ocean: implications for late to middle Pleistocene glacial history. *Climate of the Past 13*, 511–531.

Dong, L., Polyak, L., Liu, Y., Shi, X., Zhang, J. & Huang, Y. 2020: Isotopic fingerprints of ice-rafted debris offer new constraints on middle to late quaternary arctic circulation and glacial history. *Geochemistry, Geophysics, Geosystems 21*, e2020GC00901, https://doi.org/10.1029/2020GC009019.

Dong, L., Polyak, L., Xiao, X., Brachfeld, S., Liu, Y., Shi, X., Fang, X., Bai, Y., Zhu, A., Li, C. & Zhao, S. 2022: A Eurasian Basin sedimentary record of glacial impact on the central Arctic Ocean during MIS 1–4. *Global and Planetary Change 219*, 103993, https://doi.org/10.1016/j.gloplacha.2022.103993.

Dove, D., Polyak, L. & Coakley, B. 2014: Widespread, multi-source glacial erosion on the Chukchi margin, Arctic Ocean. *Quaternary Science Reviews 92*, 112–122.

Dowdeswell, J. A. & Jeffries, M. O. 2017: Arctic ice shelves: an introduction. *In* Copland, L. & Mueller, D. (eds.): *Arctic Ice Shelves and Ice Islands*, 3–21. Springer Polar Sciences, Dordrecht.

Dowdeswell, J. A., Elverhøi, A., Andrews, J. T. & Hebbeln, D. 1999: Asynchronous deposition of ice-rafted layers in the Nordic seas and North Atlantic Ocean. *Nature 400*, 348–351.

Engels, J. L., Edwards, M. H., Polyak, L. & Johnson, P. D. 2008: Seafloor evidence for ice shelf flow across the Alaska–Beaufort margin of the Arctic Ocean. *Earth Surface Processes and Landforms 33*, 1047–1063.

Fagel, N., Not, C., Gueibe, J., Mattielli, N. & Bazhenova, E. 2014: Late quaternary evolution of sediment provenances in the central Arctic Ocean: mineral assemblage, trace element composition and Nd and Pb isotope fingerprints of detrital fraction from the northern Mendeleev Ridge. *Quaternary Science Reviews 92*, 140–154.

Farmer, J. R., Pico, T., Underwood, O. M., Cleveland Stout, R., Granger, J., Cronin, T. M., Fripiat, F., Martínez-García, A., Haug, G. H. & Sigman, D. M. 2023: The Bering Strait was flooded 10,000 years before the Last Glacial Maximum. *Proceedings of the National Academy of Sciences of the United States of America 120*, e2206742119, https://doi.org/10.1073/pnas.2206742119.

Gariépy, C., Ghaleb, B., Hillaire-Marcel, C., Mucci, A. & Vallieres, S. 1994: Early diagenetic processes in Labrador Sea sediments: uranium-isotope geochemistry. *Canadian Journal of Earth Sciences 31*, 28–37.

Gasson, E. G., DeConto, R. M., Pollard, D. & Clark, C. D. 2018: Numerical simulations of a kilometre-thick Arctic ice shelf consistent

with ice grounding observations. *Nature Communications 9*, 1510, https://doi.org/10.1038/s41467-018-03707-w.
Geibert, W., Matthiessen, J., Stimac, I., Wollenburg, J. & Stein, R. 2021: Glacial episodes of a freshwater Arctic Ocean covered by a thick ice shelf. *Nature 590*, 97–102.
Geibert, W., Matthiessen, J., Wollenburg, J. & Stein, R. 2022: Reply to 'Challenging the hypothesis of an arctic ocean lake during recent glacial episodes' by Hillaire-Marcel, *et al*. *Journal of Quaternary Science 37*, 568–571.
Grosswald, M. G. & Hughes, T. J. 1999: The case for an ice shelf in the Pleistocene Arctic Ocean. *Polar Geography 23*, 23–54.
Gualtieri, L., Vartanyan, S., Brigham-Grette, J. & Anderson, P. M. 2003: Pleistocene raised marine deposits on Wrangel Island, Northeast Siberia and implications for the presence of an East Siberian ice sheet. *Quaternary Research 59*, 399–410.
Guballa, J. D. & Peleo-Alampay, A. M. 2020: Pleistocene calcareous nannofossil biostratigraphy and gephyrocapsid occurrence in site U1431D, IODP 349, South China Sea. *Geosciences 10*, 388, https://doi.org/10.3390/geosciences10100388.
Gusev, E. A., Maksimov, F. E., Kuznetsov, V. Y., Basov, V. A., Novikhina, E. S., Kupriyanova, N. V., Levchenko, S. B. & Zherebtsov, I. E. 2013: Stratigraphy of bottom sediments in the Mendeleev Ridge area (Arctic Ocean). *Doklady Akademii Nauk 450*, 602–606.
Hanslik, D., Löwemark, L. & Jakobsson, M. 2013: Biogenic and detrital-rich intervals in central Arctic Ocean cores identified using X-ray fluorescence scanning. *Polar Research 32*, 18386, https://doi.org/10.3402/polar.v32i0.18386.
Haynert, K., Schönfeld, J., Riebesell, U. & Polovodova, I. 2011: Biometry and dissolution features of the benthic foraminifer *Ammonia aomoriensis* at high pCO_2. *Marine Ecology Progress Series 432*, 53–67.
Hayward, B. W., Grenfell, H. R., Carter, R. & Hayward, J. J. 2004: Benthic foraminiferal proxy evidence for the Neogene palaeoceanographic history of the Southwest Pacific, east of New Zealand. *Marine Geology 205*, 147–184.
Herman, Y. 1970: Arctic paleo-oceanography in late Cenozoic time. *Science 169*, 474–477.
Hillaire-Marcel, C. & de Vernal, A. 2022: A comment about "A sedimentary record from the Makarov Basin, Arctic Ocean, reveals changing middle to late Pleistocene glaciation patterns" (Quat. Sci. Rev., 270 (2021), p. 107176) from W. Xiao, L. Polyak, R. Wang, C. Not, L. Dong, Y. Liu, T. Ma, T. Zhang. *Quaternary Science Reviews 279*, 107239, https://doi.org/10.1016/j.quascirev.2021.107239.
Hillaire-Marcel, C., Ghaleb, B., de Vernal, A., Maccali, J., Cuny, K., Jacobel, A., Le Duc, C. & McManus, J. 2017: A new chronology of late Quaternary sequences from the central Arctic Ocean based on "extinction ages" of their excesses in ^{231}Pa and ^{230}Th. *Geochemistry, Geophysics, Geosystems 18*, 4573–4585, https://doi.org/10.1002/2017GC007050.
Hillaire-Marcel, C., Myers, P. G., Marshall, S., Tarasov, L., Purcell, K., Not, C. & de Vernal, A. 2022a: Challenging the hypothesis of an Arctic Ocean lake during recent glacial episodes. *Journal of Quaternary Science 37*, 559–567.
Hillaire-Marcel, C., de Vernal, A. & Crucifix, M. 2021: Sea-level and summer season orbital insolation as drivers of Arctic sea-ice. *arXiv 2102*, 02067, https://doi.org/10.48550/arXiv.2102.02067.
Hillaire-Marcel, C., de Vernal, A., Rong, Y., Roberge, P. & Song, T. 2022b: Challenging radiocarbon chronostratigraphies in central Arctic Ocean sediment. *Geophysical Research Letters 49*, e2022GL100446, https://doi.org/10.1029/2022GL100446.
Huh, C. A., Pisias, N. G., Kelley, J. M., Maiti, T. C. & Grantz, A. 1997: Natural radionuclides and plutonium in sediments from the western Arctic Ocean: sedimentation rates and pathways of radionuclides. *Deep Sea Research Part II: Topical Studies in Oceanography 44*, 1725–1743.
Jakobsson, M., Grantz, A., Kristoffersen, Y. & Macnab, R. 2003: Physiographic provinces of the Arctic Ocean seafloor. *Geological Society of America Bulletin 115*, 1443–1455.
Jakobsson, M., Løvlie, R., Al-Hanbali, H., Arnold, E., Backman, J. & Mörth, M. 2000: Manganese and color cycles in Arctic Ocean sediments constrain Pleistocene chronology. *Geology 28*, 23–26.
Jakobsson, M., Løvlie, R., Arnold, E. M., Backman, J., Polyak, L., Knutsen, J. O. & Musatov, E. 2001: Pleistocene stratigraphy and paleoenvironmental variation from Lomonosov Ridge sediments, central Arctic Ocean. *Global and Planetary Change 31*, 1–22. https://doi.org/10.1016/S0921-8181(01)00110-2.
Jakobsson, M., Nilsson, J., Anderson, L., Backman, J., Björk, G., Cronin, T. M., Kirchner, N., Koshurnikov, A., Mayer, L., Noormets, R. & O'Regan, M. 2016: Evidence for an ice shelf covering the central Arctic Ocean during the penultimate glaciation. *Nature Communications 7*, 10365, https://doi.org/10.1038/ncomms10365.
Jakobsson, M., Nilsson, J., O'Regan, M., Backman, J., Löwemark, L., Dowdeswell, J. A., Mayer, L., Polyak, L., Colleoni, F., Anderson, L. G. & Björk, G. 2010: An Arctic Ocean ice shelf during MIS 6 constrained by new geophysical and geological data. *Quaternary Science Reviews 29*, 3505–3517.
Jakobsson, M., Polyak, L., Edwards, M., Kleman, J. & Coakley, B. 2008: Glacial geomorphology of the central Arctic Ocean: the Chukchi Borderland and the Lomonosov Ridge. *Earth Surface Processes and Landforms 33*, 526–545.
Jennings, A., Reilly, B., Andrews, J., Hogan, K., Walczak, M., Jakobsson, M., Stoner, J., Mix, A., Nicholls, K. W., O'Regan, M. & Prins, M. A. 2022: Modern and early Holocene ice shelf sediment facies from Petermann Fjord and northern Nares Strait, northwest Greenland. *Quaternary Science Reviews 283*, 107460, https://doi.org/10.1016/j.quascirev.2022.107460.
Joe, Y. J., Polyak, L., Schreck, M., Niessen, F., Yoon, S. H., Kong, G. S. & Nam, S. I. 2020: Late Quaternary depositional and glacial history of the Arliss Plateau off the East Siberian margin in the western Arctic Ocean. *Quaternary Science Reviews 228*, 106099, https://doi.org/10.1016/j.quascirev.2019.106099.
Kageyama, M., Harrison, S. P., Kapsch, M. L., Lofverstrom, M., Lora, J. M., Mikolajewicz, U., Sherriff-Tadano, S., Vadsaria, T., Abe-Ouchi, A., Bouttes, N. & Chandan, D. 2021: The PMIP4 Last Glacial Maximum experiments: preliminary results and comparison with the PMIP3 simulations. *Climate of the Past 17*, 1065–1089.
Kim, S., Polyak, L., Joe, Y. J., Niessen, F., Kim, H. J., Choi, Y., Kang, S. G., Hong, J. K., Nam, S. I. & Jin, Y. K. 2021: Seismostratigraphic and geomorphic evidence for the glacial history of the northwestern Chukchi margin, Arctic Ocean. *Journal of Geophysical Research: Earth Surface 126*, e2020JF006030, https://doi.org/10.1029/2020JF006030.
Kleman, J. & Applegate, P. J. 2014: Durations and propagation patterns of ice sheet instability events. *Quaternary Science Reviews 92*, 32–39.
Koo, H., Jin, Y. & Cho, H. 2021: Change in sediment provenance on the inner slope of the Chukchi Rise and their paleoenvironmental implications. *Applied Sciences 11*, 6491, https://doi.org/10.3390/app11146491.
Kremer, A., Stein, R., Fahl, K., Ji, Z., Yang, Z., Wiers, S., Matthiessen, J., Forwick, M., Löwemark, L., O'Regan, M. & Chen, J. 2018: Changes in sea ice cover and ice sheet extent at the Yermak plateau during the last 160 ka – reconstructions from biomarker records. *Quaternary Science Reviews 182*, 93–108.
Le Duc, C. 2018: *Flux sédimentaires le long de la ride de Lomonosov, ocean arctique*. Mémoire M.Sc., UQAM, 49 pp.
Lisitzin, A. P. 2002: *Sea-Ice and Iceberg Sedimentation in the Ocean: Recent and Past*. 563 pp. Springer-Verlag, Berlin.
Liu, J., Shi, X., Liu, Y., Liu, Q., Liu, Y., Zhang, Q., Ge, S. & Li, J. 2019: A thick negative polarity anomaly in a sediment core from the central arctic ocean: geomagnetic excursion versus reversal. *Journal of Geophysical Research: Solid Earth 124*, 10687–10703, https://doi.org/10.1029/2019JB018073.
Macdonald, R. W. & Gobeil, C. 2012: Manganese sources and sinks in the Arctic Ocean with reference to periodic enrichments in basin sediments. *Aquatic Geochemistry 18*, 565–591.
McManus, J., Berelson, W. M., Klinkhammer, G. P., Hammond, D. E. & Holm, C. 2005: Authigenic uranium: relationship to oxygen penetration depth and organic carbon rain. *Geochimica et Cosmochimica Acta 69*, 95–108.
deMenocal, P. B., Ruddiman, W. F. & Kent, D. V. 1990: Depth of post-depositional remanence acquisition in deep-sea sediments: a case study of the Brunhes-Matuyama reversal and oxygen isotopic stage 19.1. *Earth and Planetary Science Letters 99*, 1–13.

Miller, G. H., Alley, R. B., Brigham-Grette, J., Fitzpatrick, J. J., Polyak, L., Serreze, M. C. & White, J. W. 2010: Arctic amplification: can the past constrain the future? *Quaternary Science Reviews 29*, 1779–1790.

Niessen, F., Hong, J. K., Hegewald, A., Matthiessen, J., Stein, R., Kim, H., Kim, S., Jensen, L., Jokat, W., Nam, S. I. & Kang, S. H. 2013: Repeated Pleistocene glaciation of the East Siberian continental margin. *Nature Geoscience 6*, 842–846.

Nørgaard, J., Margold, M., Jansen, J. D., Kurbanov, R., Szuman, I., Andersen, J. L., Olsen, J. & Knudsen, M. F. 2023: Absence of large-scale ice masses in central Northeast Siberia during the late Pleistocene. *Geophysical Research Letters 50*, e2023GL103594, https://doi.org/10.1029/2023GL103594.

Nørgaard-Pedersen, N., Mikkelsen, N. & Kristoffersen, Y. 2007: Arctic Ocean record of last two glacial-interglacial cycles off North Greenland/Ellesmere Island—implications for glacial history. *Marine Geology 244*, 93–108.

Not, C. & Hillaire-Marcel, C. 2010: Time constraints from ^{230}Th and ^{231}Pa data in late Quaternary, low sedimentation rate sequences from the Arctic Ocean: an example from the northern Mendeleev Ridge. *Quaternary Science Reviews 29*, 3665–3675.

Not, C. & Hillaire-Marcel, C. 2012: Enhanced sea-ice export from the Arctic during the Younger Dryas. *Nature Communications 3*, 647, https://doi.org/10.1038/ncomms1658.

Not, C., Brown, K., Ghaleb, B. & Hillaire-Marcel, C. 2012: Conservative behavior of uranium vs. salinity in Arctic sea ice and brine. *Marine Chemistry 130*, 33–39.

Not, C., Hillaire-Marcel, C., Ghaleb, B., Polyak, L. & Darby, D. 2008: ^{210}Pb–^{226}Ra–^{230}Th systematics in very low sedimentation rate sediments from the Mendeleev Ridge (Arctic Ocean). *Canadian Journal of Earth Sciences 45*, 1207–1219.

O'Regan, M., Backman, J., Barrientos, N., Cronin, T. M., Gemery, L., Kirchner, N., Mayer, L. A., Nilsson, J., Noormets, R., Pearce, C. & Semiletov, I. 2017: The De long trough: a newly discovered glacial trough on the East Siberian continental margin. *Climate of the Past 13*, 1269–1284.

Park, K., Ohkushi, K. I., Cho, H. G. & Khim, B. K. 2017: Lithostratigraphy and paleoceanography in the Chukchi Rise of the western Arctic Ocean since the last glacial period. *Polar Science 11*, 42–53.

Park, K., Wang, R., Xiao, W., Polyak, L., Cho, H. G. & Khim, B. K. 2022: Increased terrigenous input from North America to the northern Mendeleev Ridge (Western Arctic Ocean) since the mid-Brunhes Event. *Scientific Reports 12*, 15189, https://doi.org/10.1038/s41598-022-19082-y.

Polyak, L. & Jakobsson, M. 2011: Quaternary sedimentation in the Arctic Ocean: recent advances and further challenges. *Oceanography 24*, 52–64.

Polyak, L., Alley, R. B., Andrews, J. T., Brigham-Grette, J., Cronin, T. M., Darby, D. A., Dyke, A. S., Fitzpatrick, J. J., Funder, S., Holland, M. & Jennings, A. E. 2010: History of sea ice in the Arctic. *Quaternary Science Reviews 29*, 1757–1778.

Polyak, L., Bischof, J., Ortiz, J. D., Darby, D. A., Channell, J. E., Xuan, C., Kaufman, D. S., Løvlie, R., Schneider, D. A., Eberl, D. D. & Adler, R. E. 2009: Late Quaternary stratigraphy and sedimentation patterns in the western Arctic Ocean. *Global and Planetary Change 68*, 5–17.

Polyak, L., Curry, W. B., Darby, D. A., Bischof, J. & Cronin, T. M. 2004: Contrasting glacial/interglacial regimes in the western Arctic Ocean as exemplified by a sedimentary record from the Mendeleev Ridge. *Palaeogeography, Palaeoclimatology, Palaeoecology 203*, 73–93.

Polyak, L., Edwards, M. H., Coakley, B. J. & Jakobsson, M. 2001: Ice shelves in the Pleistocene Arctic Ocean inferred from glaciogenic deep-sea bedforms. *Nature 410*, 453–457.

Purcell, K., Hillaire-Marcel, C., de Vernal, A., Ghaleb, B. & Stein, R. 2022: Potential and limitation of ^{230}Th-excess as a chronostratigraphic tool for late Quaternary Arctic Ocean sediment studies: an example from the southern Lomonosov Ridge. *Marine Geology 448*, 106802, https://doi.org/10.1016/j.margeo.2022.106802.

Reilly, B. T., Natter, C. J., Jr. & Brachfeld, S. A. 2016: Holocene glacial activity in Barilari Bay, west Antarctic Peninsula, tracked by magnetic mineral assemblages: linking ice, ocean, and atmosphere. *Geochemistry, Geophysics, Geosystems 17*, 4553–4565.

Reimnitz, E., Kempema, E. W. & Barnes, P. W. 1987: Anchor ice, seabed freezing, and sediment dynamics in shallow Arctic seas. *Journal of Geophysical Research: Oceans 92*, 14671–14678.

Rogalla, B., Allen, S. E., Colombo, M., Myers, P. G. & Orians, K. J. 2022: Sediments in sea ice drive the Canada Basin surface Mn maximum: insights from an Arctic Mn ocean model. *Global Biogeochemical Cycles 36*, e2022GB007320, https://doi.org/10.1029/2022GB007320.

Schreck, M., Nam, S. I., Polyak, L., Vogt, C., Kong, G. S., Stein, R., Matthiessen, J. & Niessen, F. 2018: Improved Pleistocene sediment stratigraphy and paleoenvironmental implications for the western Arctic Ocean off the East Siberian and Chukchi margins. *Arktos 4*, 21, https://doi.org/10.1007/s41063-018-0057-8.

Schubert, C. J. & Calvert, S. E. 2001: Nitrogen and carbon isotopic composition of marine and terrestrial organic matter in Arctic Ocean sediments: implications for nutrient utilization and organic matter composition. *Deep Sea Research Part I: Oceanographic Research Papers 48*, 789–810.

Schulz, K., Büttner, S., Rogge, A., Janout, M., Hölemann, J. & Rippeth, T. P. 2021: Turbulent mixing and the formation of an intermediate nepheloid layer above the Siberian continental shelf break. *Geophysical Research Letters 48*, e2021GL092988, https://doi.org/10.1029/2021GL092988.

Sher, A. 1995: Is there any real evidence for a huge shelf ice sheet in East Siberia? *Quaternary International 28*, 39–40.

Siddall, M., Rohling, E. J., Thompson, W. G. & Waelbroeck, C. 2008: Marine isotope stage 3 sea level fluctuations: data synthesis and new outlook. *Reviews of Geophysics 46*, RG4003, https://doi.org/10.1029/2007RG000226.

Song, T., Hillaire-Marcel, C., de Vernal, A., Liu, Y., Wang, W. & Huang, Y. 2022: A reassessment of Nd-isotopes and clay minerals as tracers of the Holocene Pacific water flux through Bering Strait. *Marine Geology 443*, 106698, https://doi.org/10.1016/j.margeo.2021.106698.

Spielhagen, R. F., Baumann, K. H., Erlenkeuser, H., Nowaczyk, N. R., Nørgaard-Pedersen, N., Vogt, C. & Weiel, D. 2004: Arctic Ocean deep-sea record of northern Eurasian ice sheet history. *Quaternary Science Reviews 23*, 1455–1483.

Spielhagen, R. F., Bonani, G., Eisenhauer, A., Frank, M., Frederichs, T., Kassens, H., Kubik, P. W., Mangini, A., Nøgaard Pedersen, N., Nowaczyk, N. R. & Schäper, S. 1997: Arctic Ocean evidence for late Quaternary initiation of northern Eurasian ice sheets. *Geology 25*, 783–786.

Stein, R. 2008: Arctic Ocean sediments: processes, proxies, and paleoenvironment. *In* Chamley, H. (ed.): *Developments in Marine Geology*, 142–146. Elsevier, Oxford.

Stein, R., Fahl, K., Gierz, P., Niessen, F. & Lohmann, G. 2017: Arctic Ocean sea ice cover during the penultimate glacial and the last interglacial. *Nature Communications 8*, 373, https://doi.org/10.1038/s41467-017-00552-1.

Strobl, C. 1998: *Datierung von Sedimentkernen und Rekonstruktion der Transportwege der Radionuklide ^{10}Be, ^{230}Th und ^{231}Pa in hohen nördlichen Breiten*. Ph.D. thesis, Universität Heidelberg, 183 pp.

Sundby, B., Lecroart, P., Anschutz, P., Katsev, S. & Mucci, A. 2015: When deep diagenesis in Arctic Ocean sediments compromises manganese-based geochronology. *Marine Geology 366*, 62–68.

Swärd, H., Andersson, P., Hilton, R., Vogt, C. & O'Regan, M. 2022: Mineral and isotopic (Nd, Sr) signature of fine-grained deglacial and Holocene sediments from the Mackenzie Trough, Arctic Canada. *Arctic, Antarctic, and Alpine Research 54*, 346–367.

Thierstein, H. R., Geitzenauer, K. R., Molfino, B. & Shackleton, N. J. 1977: Global synchroneity of late Quaternary coccolith datum levels: validation by oxygen isotopes. *Geology 5*, 400–404.

Thomson, W. 1888: Polar ice-caps and their influence in changing sea levels. *Transactions of the Geological Society of Glasgow 8*, 322–340.

Tzevahirtzian, A., Caruso, A., Andreetto, F., Bonomo, S. & Krijgsman, W. 2023: A bio-chronostratigraphic study of the upper Miocene from the northern Caltanissetta Basin, Sicily (core 3AGN2S04). Implications for dating the Messinian salinity crisis onset. *Sedimentary Geology 445*, 106330, https://doi.org/10.1016/j.sedgeo.2023.106330.

Tziperman, E. & Gildor, H. 2003: On the mid-Pleistocene transition to 100-kyr glacial cycles and the asymmetry between glaciation and deglaciation times. *Paleoceanography 18*, 1001, https://doi.org/10.1029/2001pa000627.

de Vernal, A., Hillaire-Marcel, C., Le Duc, C., Roberge, P., Brice, C., Matthiessen, J., Spielhagen, R. F. & Stein, R. 2020: Natural variability of the Arctic Ocean sea ice during the present interglacial. *Proceedings of the National Academy of Sciences of the United States of America 117*, 26069–26075.

Viscosi-Shirley, C., Mammone, K., Pisias, N. & Dymond, J. 2003: Clay mineralogy and multi-element chemistry of surface sediments on the Siberian-Arctic shelf: implications for sediment provenance and grain size sorting. *Continental Shelf Research 23*, 1175–1200.

Vogt, C. 1997: *Zeitliche und räumliche Verteilung von Mineralvergesellschaftungen in spätquartären Sedimenten des Arktischen Ozeans und ihre Nützlichkeit als Klimaindikatoren während der Glazial/Interglazial-Wechsel*. 251 pp. Berichte zur Polarforschung, AWI, Bremerhaven.

Wahsner, M., Müller, C., Stein, R., Ivanov, G., Levitan, M., Shelekhova, E. & Tarasov, G. 1999: Clay-mineral distribution in surface sediments of the Eurasian Arctic Ocean and continental margin as indicator for source areas and transport pathways – a synthesis. *Boreas 28*, 215–233.

Wall, J. D. & Krumholz, L. R. 2006: Uranium reduction. *Annual Review of Microbiology 60*, 149–166.

Wang, R., Polyak, L., Zhang, W., Yu, X., Ye, L., Dong, L., Liu, Y., Wang, W. & Diekmann, B. 2021: Glacial-interglacial sedimentation and paleocirculation at the Northwind Ridge, western Arctic Ocean. *Quaternary Science Reviews 258*, 106882, https://doi.org/10.1016/j.quascirev.2021.106882.

Watanabe, E., Onodera, J., Itoh, M. & Mizobata, K. 2022: Transport processes of seafloor sediment from the Chukchi shelf to the western Arctic basin. *Journal of Geophysical Research: Oceans 127*, e2021JC017958, https://doi.org/10.1029/2021JC017958.

Wetterich, S., Tumskoy, V., Rudaya, N., Kuznetsov, V., Maksimov, F., Opel, T., Meyer, H., Andreev, A. A. & Schirrmeister, L. 2016: Ice complex permafrost of MIS5 age in the Dmitry Laptev Strait coastal region (East Siberian Arctic). *Quaternary Science Reviews 147*, 298–311.

Wiers, S., Snowball, I., O'Regan, M., Pearce, C. & Almqvist, B. 2020: The Arctic Ocean manganese cycle, an overlooked mechanism in the anomalous palaeomagnetic sedimentary record. *Frontiers in Earth Science 8*, 75, https://doi.org/10.3389/feart.2020.00075.

Xiang, Y. & Lam, P. J. 2020: Size-fractionated compositions of marine suspended particles in the western Arctic Ocean: lateral and vertical sources. *Journal of Geophysical Research: Oceans 125*, e2020JC016144, https://doi.org/10.1029/2020JC016144.

Xiao, W., Polyak, L., Wang, R., Löwemark, L., Mei, J., You, D., Wang, W., Wu, L. & Jin, X. 2020: Middle to late Pleistocene Arctic paleoceanographic changes based on sedimentary records from Mendeleev Ridge and Makarov Basin. *Quaternary Science Reviews 228*, 106105, https://doi.org/10.1016/j.quascirev.2019.106105.

Xu, Q., Xiao, W., Wang, R., Süfke, F., Lippold, J. & Not, C. 2021: Driving mechanisms of sedimentary ^{230}Th and ^{231}Pa variability in the western Arctic Ocean through the last glacial cycle. *Paleoceanography and Paleoclimatology 36*, e2020PA004039, https://doi.org/10.1029/2020PA004039.

Xuan, C. & Channell, J. E. T. 2010: Origin of apparent magnetic excursions in deep-sea sediments from Mendeleev-Alpha Ridge, Arctic Ocean. *Geochemistry, Geophysics, Geosystems 11*, Q02003, https://doi.org/10.1029/2009GC002879.

Ye, L., Zhang, W., Wang, R., Yu, X. & Jin, L. 2020: Ice events along the East Siberian continental margin during the last two glaciations: evidence from clay minerals. *Marine Geology 428*, 106289, https://doi.org/10.1016/j.margeo.2020.106289.

Zamelczyk, K., Fransson, A., Chierici, M., Jones, E., Meilland, J., Anglada-Ortiz, G. & Hodal Lødemel, H. 2021: Distribution and abundances of planktic foraminifera and shelled pteropods during the polar night in the sea-ice covered northern Barents Sea. *Frontiers in Marine Science 8*, 644094, https://doi.org/10.3389/fmars.2021.644094.

Zhao, S., Liu, Y., Dong, L., Shi, X., Polyak, L., Zou, X., Wang, W. & Wu, D. 2022: Sedimentary record of glacial impacts and meltwater discharge off the East Siberian Continental Margin, Arctic Ocean. *Journal of Geophysical Research: Oceans 127*, e2021JC0176, https://doi.org/10.1029/2021JC017650.

Supporting Information

Additional Supporting Information to this article is available at http://www.boreas.dk.

Fig. S1. Correlation between calcite content and foraminifera abundance in core E25.

Fig. S2. ^{238}U/^{232}Th ratio vs. ^{232}Th content. Red dots = our studied core E25; blue squares = site HU2008-029-016PC from Nuttin & Hillaire-Marcel (2015); black cross = mean continental lithosphere from Wedepohl (1995).

Fig. S3. AR(^{238}U/^{232}Th) value vs. IRD and quartz contents.

Fig. S4. Linear correlation of ln(A^{230}Th) and core depth of site MA01 from Xu *et al.* (2021). Red dots = ln (A^{230}Th); blue dots = ln(A^{234}U). The calculation of extinction depth and age of $^{230}Th_{xs}$ can be found in the main text. The $^{230}Th_{xs}$ decay downcore illustrates an age of ~422±58 ka at the core depth of ~89±23 cm, suggesting that the $^{230}Th_{xs}$ peak at ~80 cm should be assigned to MIS 11 (Fig. 6).

Fig. S5. Quartz content vs. illite/quartz ratio (left) and illite content vs. illite/quartz ratio (right).

Table S1. Summary of ^{226}Ra and ^{210}Pb measurements in core E25.

Table S2. Bulk mineralogy data of core E25.

Table S3. Sedimentology data of core E25.

Table S4. Geochemistry data of core E25.